Nuclear Inst. and Methods in Physics Research, A 1056 (2023) 168545

Contents lists available at ScienceDirect

Nuclear Inst. and Methods in Physics Research, A

journal homepage: www.elsevier.com/locate/nima

Full Length Article

Increased beam energy as a pathway towards a highly selective and high-flux MR-ToF mass separator

F.M. Maier [a,b,*], F. Buchinger [c], L. Croquette [c], P. Fischer [b], H. Heylen [a], F. Hummer [a,c], C. Kanitz [a], A.A. Kwiatkowski [h], V. Lagaki [a], S. Lechner [a,c], E. Leistenschneider [a], G. Neyens [a,d], P. Plattner [a,e], A. Roitman [c], M. Rosenbusch [b,f], L. Schweikhard [b], S. Sels [a], M. Vilen [a], F. Wienholtz [a,g], S. Malbrunot-Ettenauer [a,h,i]

[a] Experimental Physics Department, CERN, CH-1211, Geneva 23, Switzerland
[b] Institut für Physik, Universität Greifswald, 17487 Greifswald, Germany
[c] McGill University, Montréal, Québec, H3A 2T8, Canada
[d] Instituut voor kern- en stralingsfysica, KU Leuven, Celestijnenlaan 200D, Leuven, Belgium
[e] Universität Innsbruck, Innrain 52, 6020 Innsbruck, Austria
[f] Wako Nuclear Science Center (WNSC), Institute of Particle and Nuclear Studies (IPNS), High Energy Accelerator Research Organization (KEK), Wako Saitama, 351-0198, Japan
[g] Institut für Kernphysik, Technische Universität Darmstadt, Schlossgartenstr. 9, 64289 Darmstadt, Germany
[h] TRIUMF, 4004 Wesbrook Mall, Vancouver, BC V6T 2A3, Canada
[i] Department of Physics, University of Toronto, 60 St. George St., Toronto, Ontario, Canada

ARTICLE INFO

Keywords:
MR-ToF device
Short-lived radionuclides
MIRACLS
Electrostatic ion beam traps
Mass separation
Space charge

ABSTRACT

Many experiments at radioactive ion beam (RIB) facilities suffer from isobaric contamination, i.e. unwanted ions of similar mass. During the last decade, Multi-Reflection Time-of-Flight (MR-ToF) devices have gained remarkable attention for mass separation of short-lived, low-intensity beams of radionuclides at RIB facilities throughout the world. They exceed mass resolving powers $m/\Delta m$ of 10^5 within a processing time of some (tens of) milliseconds. Due to space-charge effects, however, the mass separation remains an experimental challenge when many ions are simultaneously confined in the MR-ToF device. This limits the wider application of MR-ToF mass separators at RIB facilities. By performing ion-optical simulations including space-charge effects, we investigate different schemes of ion preparation in a Paul trap upstream of the MR-ToF device as well as MR-ToF operation and study their influence on mass separation and maximal ion flux. The validity of these simulations are benchmarked by time-of-flight and collision-induced fluorescence measurements with a 1.5 keV MR-ToF device. More advanced ion-beam preparation techniques such as the use of laser cooling, buffer-gas cooling at cryogenic temperatures or specific electric-field parameters for ion trapping and ejection from the Paul trap can significantly reduce the processing time needed to reach a given mass resolving power. However, the simulations of these methods also indicate that space-charge effects in the MR-ToF device become relevant at lower ion numbers compared to 'standard' ion preparation. Thus, the overall amount of mass separated ions per unit of time remains essentially the same. In contrast, the simulations suggest that increasing the kinetic energy of typically just a few kiloelectronvolts in present MR-ToF instruments to 30 keV results in a significant increase of the attainable maximal ion flux.

1. Introduction

Many experiments at radioactive ion beam (RIB) facilities require pure ion beams with high intensity. Existing mass separators, such as the high-resolution mass separator at ISOLDE/CERN [1], use dipole magnets and achieve mass resolving powers $R = m/\Delta m$ on the order of a few 1000. Next-generation magnetic mass separators such as the high-resolution isobar separator for the CARIBU project [2,3], the SPIRAL2/DESIR high resolution mass separator [4,5] or the CANREB high-resolution separator at TRIUMF [6] are in the process of reaching mass resolving powers of up to 20,000–30,000. There remain, however, many applications which require an even higher mass resolving power to suppress isobaric contamination, i.e. unwanted ions of similar mass.

Recently, Multi-Reflection Time-of-Flight (MR-ToF) devices have significantly gained in importance for the mass separation of short-lived radionuclides at RIB facilities throughout the world [7–17]. Since

* Corresponding author at: Experimental Physics Department, CERN, CH-1211, Geneva 23, Switzerland.
E-mail address: franziska.maria.maier@cern.ch (F.M. Maier).

https://doi.org/10.1016/j.nima.2023.168545
Received 31 March 2023; Received in revised form 12 July 2023; Accepted 12 July 2023
Available online 4 August 2023

they exceed mass resolving powers R of 10^5 within just some (tens of) milliseconds they are capable of providing isobaric-purified ion beams to subsequent experiments. In an MR-ToF device ions are separated in time-of-flight (ToF) according to their mass-over-charge ratio m/q. Compared to conventional ToF separation, the high mass resolving power is achieved as ion bunches bounce back and fourth between two electrostatic mirrors. Hence, a flight path of several kilometers is realized while the ions are confined in a table-top instrument. MR-ToF mass separation at high R is, however, only possible up to a limited number of ions. At large ion densities, the Coulomb interactions between the ions can no longer be neglected and, thus, so-called space-charge effects degrade the otherwise superb mass separation capabilities. In particular, phenomena such as selfbunching [18–25] and peak coalescence [22,25–27] at increased numbers of stored ions were reported in MR-ToF devices. As a consequence, the ion species do not separate in m/q any longer when too many ions are simultaneously confined.

However, virtually all fields of rare isotope science pursued at low-energy branches of RIB facilities would benefit from isobaric pure beams with a high ion intensity. For some initiatives such as the antiProton Unstable Matter Annihilation (PUMA) project [28] for the study of the interaction of anti-matter with radioactive nuclides, pure radioactive ion beams are an indispensable prerequisite. Even applications closer to stability like the production of innovative medical isotopes [29,30] suffer from isobaric contamination, including molecular isobars. An advanced beam purification apparatus with a large ion flux could reduce the need of chemical separation and would hence reduce the radioactive activity during transport and handling as well as the radioactive waste.

Magnetic separators are expected to continue exceeding MR-ToF systems in ion flux while the latter remain superior in attainable mass resolving power. The ultimate configuration would, thus, combine mass separation in stages in which a high resolution magnetic separator delivers a 'pre-separated' RIB to an MR-ToF device ideally with a higher ion throughput compared to current state-of-the-art MR-ToF instruments. Magnetic dipole separation and MR-ToF separation differ in their time structure of operation. While magnetic mass separators work for a continuous beam of ions, a bunched beam structure is required for MR-ToF operation, see below.

Employing ion optical simulations including ion–ion interactions, the present work investigates options to increase the mass resolving power of MR-ToF devices and the maximal ion flux while maintaining the large mass resolving power. Our findings suggest that, while the ion preparation in a cooler-buncher prior to the MR-ToF device has for most applications no significant influence on the maximal ion flux possible at a given resolving power, increasing the kinetic energy of the stored ions from 1.5 keV to 30 keV could substantially increase the number of mass separated ions per unit of time.

To benchmark the validity of the simulation approach, time-of-flight studies of ion bunches extracted from the MR-ToF device as well as collisional-induced fluorescence measurements with a 1.5 keV MR-ToF device [24,26,27,31,35,36] are carried out. For the latter, we take advantage of inelastic collisions between ions and residual gas particles leading to fluorescence [24,37]. The detection of the emitted photons enables the tracking of the evolution of the ion bunch's temporal spread over revolution number [24] and thereby understand the ion dynamics within the MR-ToF device for varying numbers of stored ions.

The next section introduces general characteristics of MR-ToF systems and Section 3 describes the experimental setup consisting of a 1.5 keV MR-ToF device used for benchmarking the simulation code. In Section 4 the simulated mass resolving power is compared with and validated by the experimental one. Afterwards the simulation code is employed to investigate the advantages of a 30 keV MR-ToF mass separator in the context of single-ion counting experiments where ion–ion interactions are negligible. In Section 5 space-charge effects are taken into account between the ensemble of one single ion species and between two different ion species. The simulation results are benchmarked against the collisional excitation data from the 1.5 keV MR-ToF device. In Section 6 we study the ion flux in MR-ToF devices and explore and simulate different possibilities to increase it. Section 7 finally introduces a novel 30 keV MR-ToF mass separator with significantly higher ion throughput, which is currently under construction at ISOLDE/CERN as part of the MIRACLS project.

2. General characteristics of MR-ToF systems

Typically an MR-ToF system consists of a Paul trap forming bunched beams, some injection optics and the MR-ToF device itself (see Fig. 1). After some revolutions within the confining electrostatic fields in the MR-ToF device the ions are ejected onto a downstream detector either by lowering the potentials of the mirror electrodes or by raising the kinetic energy of the ions via the technique of in-trap lift switching [38].

Important performance characteristics are mass resolving power, processing time and maximal ion flux. The mass resolving power $R = m/\Delta m$ (also see Eq. (2)) describes the capability of the device to mass separate two ion species with masses m_1 and m_2.

The processing time t_{proc} describes how long it takes to mass separate the stored ions, so the needed time until a given mass resolving power is reached. It is a sum of the preparation time t_{prep} of the ion bunch in the Paul trap (typically 2 ms) and the storage time t_s in the MR-ToF device required to achieve the desired mass separation (typically a few (tens of) milliseconds). In case of parallel preparation of an ion bunch in the Paul trap and mass separation of another ion bunch in the MR-ToF device t_{proc} is given by $\max(t_s, t_{\mathrm{prep}})$.

For the following, the maximal ion flux ϕ is defined by the number of ions which can be mass separated per unit of time,

$$\phi = \frac{N_{\max}}{t_{\mathrm{proc}}} = \frac{N_{\max}}{\max(t_s, t_{\mathrm{prep}})}. \tag{1}$$

It is limited by the processing time t_{proc} as well as by the maximal ion number $N_{\max}$ that can be confined simultaneously in the MR-ToF device without notable space-charge effects between the ions due to repulsive Coulomb interactions.

At the detector plane the mass resolving power follows [12]

$$R = \frac{m}{\Delta m} = \frac{t}{2\Delta t} = \frac{t_0 + rt_1 + t_d}{2\sqrt{\Delta t_0^2 + (r\Delta t_1)^2}}, \tag{2}$$

where t is the ions' total flight time upon extraction from the Paul trap and Δt is the temporal spread of the ion bunch at the detector. The total flight time t is the sum of the time t_0 required to transport the ions from the Paul trap to the middle of the MR-ToF device, the storage time $t_s = rt_1$, and the time t_d the ions travel from the middle of the MR-ToF device to the ion detector after ejection. r is the number of revolutions and t_1 is the duration of a full revolution i.e. the period. Δt_0 is the initial bunch width when the ions pass the transversal middle plane of the MR-ToF device for the first time. Finally, Δt_1 is the ToF peak-width broadening per revolution in the MR-ToF device.

In the limit of infinite revolutions, the mass resolving power is given by $R_{\mathrm{inf}} = t_1/(2\Delta t_1)$. The initial time spread Δt_0 mainly determines the processing time, so how long it takes to reach a certain mass resolving power $R < R_{\mathrm{inf}}$. Δt, Δt_0 and Δt_1 are given as the full-width-at-half-maximum (FWHM) of the ToF peak width throughout this work.

For optimal mass separation, however, the devices' operational mass resolving power may have to be increased to $R_\beta = \beta \cdot R = \beta \cdot m/\Delta m$ where β is a factor which depends on the ToF peak shapes as well as the abundance ratios r_{ab} between the two stored ion species of mass m_1 and m_2. For perfectly Gaussian ToF peak shapes and abundance ratios r_{ab} between 1e−4 and 1e4 β lies typically between 1.5 and 3 [12]. The abundance ratio is given by $r_{\mathrm{ab}} = N_1/N_2$, where N_1 is the number of ions with mass m_1 and N_2 is the number of ions with mass m_2 with $m_2 > m_1$.

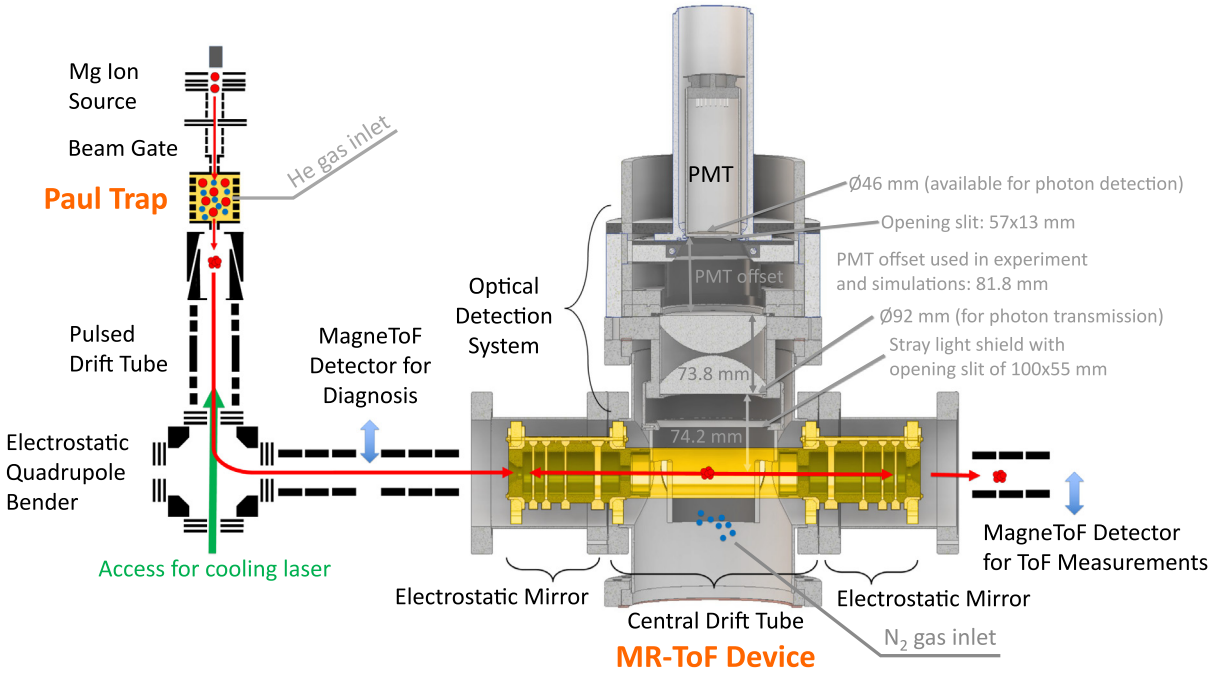

Fig. 1. Schematic overview of the MIRACLS low-energy setup at ISOLDE, which operates at 1.5 keV beam energy and takes up a floor space of around 1.5 m × 2 m. Only the MR-ToF section and the optical detection system located above the central drift tube of the MR-ToF device are to scale. The central drift tube is made out of a conductive mesh as discussed in Ref. [31]. An optical lens system, adapted from Refs. [32,33], images the collisional-induced fluorescence photons onto a photomultiplier tube (PMT). For the laser cooling measurements a second quadrupole bender was installed between the ion source and the Paul trap allowing to monitor the cooling laser passing through the Paul trap openings, see Ref. [34]. For an explanation of the ions' path see text. The dimensions stated are relevant for optical ray tracing simulations as discussed in Section 5.1.

Note that Eq. (2) strictly holds true only when the time-focus plane[1] is set close to the detector plane [38] without trapping in the MR-ToF device. In this case, starting from Δt_0, the ion bunch width is steadily increasing with revolution number caused by unwanted ion-optical aberrations. Δt_0 is given by the turn-around time in the Paul trap [13] and an additional contribution in case the time-focus point is not set exactly to the middle plane of the MR-ToF device. The mass resolving power hence increases almost linearly for the first few milliseconds, until it approaches R_{inf}.

The spatial location of the time-focus plane depends on the extraction field strength in the Paul trap. The stronger the extraction field gradient from the Paul trap, the more the time-focus point shifts closer towards the Paul trap [39]. Thus, in order to place this time-focus point close to the detector plane, as necessary for application of Eq. (2), the extraction field strength is limited to a certain range depending on the distance between Paul trap and MR-ToF device [39]. This allows to keep the potential tune of the MR-ToF mirror electrodes largely independent of the number of revolutions in the MR-ToF device. This approach is followed in the present work. Alternatively, the initial voltage of the central drift tube can be varied in the in-trap lift technique to adjust the position of the time focus onto the detector plane for each revolution number separately [38]. Moreover, the dynamical time-focus-shift technique [39] can be applied to keep the potential tune independent of the number of revolutions in the MR-ToF device.

3. Experimental setup and typical operation

In the following the MIRACLS low-energy MR-ToF setup at ISOLDE/CERN [24,31,34–36,40], a typical MR-ToF system operating at 1.5 keV beam energy, is introduced. This setup is used for the experimental studies in this work, which allow to benchmark the simulation code and to illustrate and understand important MR-ToF characteristics. Fig. 1 shows an overview of the setup. It includes an electron-impact ionization source similar to Ref. [41], producing a continuous beam of singly-charged ions of stable magnesium isotopes $^{24,25,26}Mg^+$. These ions are injected into a linear Paul trap which acts as a cooler-buncher to accumulate ions and obtain bunched beams. An electrostatic steerer upstream of the Paul trap is used as a beam gate to control the number of ions injected into the Paul trap. In the Paul trap, the ions can either be cooled by helium buffer gas at room-temperature and around 3e−6 mbar helium pressure as measured in the surrounding vacuum chamber or by performing a combination of buffer-gas and laser cooling in which the former is done with the background residual gas present in the system. If only 300 K beam temperature is required, standard buffer-gas cooling can be applied and a cooling time of 2 ms is normally sufficient, when a buffer gas pressure of around 1e−2 mbar is used in the Paul trap [34]. For Doppler cooling a continuous-wave laser beam with a wavelength of 280 nm is sent into the Paul trap. Within around 100 ms of ion-storage time in the Paul trap, the Mg^+ ions can be laser-cooled down to a few Kelvin. More details about Paul-trap operation and laser cooling in this setup are found in Ref. [34]. For ion extraction an exit endcap is switched to a lower potential. The switch time is phase locked to the radio-frequency of the Paul trap. After ion extraction from the Paul trap, the ion bunch is deflected by an electrostatic quadrupole bender onto the axis of the MR-ToF device. There, it is captured by the in-trap lift [38] and trapped for thousands of revolutions at a beam energy of around 1.5 keV. After a given storage time in the MR-ToF device, the ions are ejected (again by activating the in-trap lift [38]) and impinge on a MagneToF detector for time-of-flight measurements. Another MagneToF detector is installed in front of the MR-ToF device to allow improved diagnostics of its capture efficiency. The MR-ToF component itself consists of two opposing electrostatic mirrors and a central drift tube. Each mirror is made out of four concentric ring electrodes. The MR-ToF device has a total length of 384 mm and the central drift tube has a length of 212 mm. More details can be found in Refs. [31,35,36].

[1] The time-focus point corresponds to the moment when the faster ions, which are initially at the end of the ion bunch, overtake the slower ions, which left the Paul trap first.

For studies of the device's mass resolving power, the outermost three mirror electrodes are passively stabilized and the second outermost one is also actively stabilized. This reduces the impact of voltage fluctuations on the ions' flight time, following a similar stabilization procedure as discussed in Refs. [42,43].

For collision-induced fluorescence studies, above the central drift tube of the MR-ToF device an optical lens system adapted from Refs. [32,33] and a photomultiplier tube are mounted for detection of the emitted photons. In order to increase the collision probability of the Mg^+ ions with residual gas particles, the background pressure in the MR-ToF device can be increased to 1e−7 mbar by leaking in nitrogen gas. For this purpose, a precision needle valve is installed at the vacuum chamber close to the central drift tube.

4. Studies of the mass resolving power

4.1. Simulations of the mass resolving power

To investigate the advantages of an increased beam energy on the mass resolving power and processing time, a dedicated simulation code is developed and validated by experimental measurements of the mass resolving power as a function of the storage time t_s in MIRACLS' low-energy MR-ToF setup. The measurements are performed in single-ion counting mode where ion–ion interactions are negligible, hence space-charge effects are also neglected in the simulations. (In Section 5 Coulomb interactions will be added to the simulation code.)

The simulations targeting the mass resolving power are carried out with the software package SIMION following the procedure described in Ref. [31]. Further details about the computational requirements can be found in the Appendix. Firstly, simulations of the ion preparation in the Paul trap are performed by employing SIMION's built-in hard-sphere interaction model [44] and/or a custom-made code for Doppler cooling [34]. A thousand $^{24}Mg^+$ ions are positioned around the potential minimum of the Paul trap and left to thermalize with room-temperature or 5 K buffer-gas and/or are Doppler cooled. After extraction of the ion bunches from the Paul trap, they pass the ion optical elements and are captured in the MR-ToF device.

Each time the ions pass the middle plane of the MR-ToF device, their time-of-flight is recorded. The release of the ions from the MR-ToF device is not taken into account. It is shown for some selected settings that the time t_d the ions travel from the middle of the MR-ToF device to the ion detector after ejection can be neglected in the simulations as well as in the experiment for this particular geometry and chosen extraction field strengths.

To evaluate Eq. (2) for simulated data, the times t_0 and t_1 as well as the initial time spread Δt_0 follow directly from the simulated ion distribution. In principle, Δt after many thousands of revolutions and, thus, the peak width broadening per revolution Δt_1 would follow from the simulated ion distribution, too. In practice, however, only a few hundred revolutions can be simulated with sufficient accuracy. Computational errors occur during each ion reversal and they accumulate with every additional simulated revolution, see Ref. [45] and the Appendix. Hence the ions are studied for only up to 100 revolutions. The peak-width broadening Δt_1 over 100 revolutions is very small for optimized settings. To observe the small changes of the ion bunch width Δt over revolution number in the simulated data, the flight time of each ion in the MR-ToF device is evaluated with respect to the time the ion first crosses the transversal middle plane of the MR-ToF device. This means for the determination of the peak-width broadening Δt_1, the initial time spread Δt_0 is artificially set to zero when the ions are captured in the MR-ToF device, see also Ref. [45]. The resulting time spread Δt considering all ions after 100 revolutions is divided by the revolution number to obtain Δt_1. For a given scenario (Paul-trap operation, transfer beam line, MR-ToF mirrors) all required input values for Eq. (2) are thus extracted from the simulations and the corresponding mass resolving power is obtained.

Table 1
Potentials for the MR-ToF mirror electrodes and the in-trap lift as obtained in the optimization procedure described in the text. The in-trap lift potential needs to be readjusted for different extraction field strengths from the Paul trap.

Respective electrode	Potential (V)
Mirror electrode 1 (innermost)	−4776.6
Mirror electrode 2	1215.8
Mirror electrode 3	995.3
Mirror electrode 4 (outermost)	1881.9
In-trap lift	778.0 to 801.0

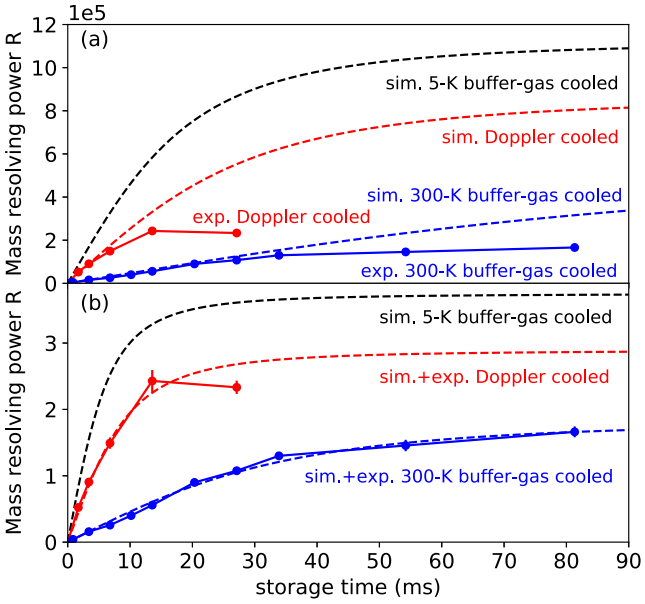

Fig. 2. Mass resolving power versus storage time for 300 K buffer gas, 5 K buffer gas and Doppler cooling for $^{24}Mg^+$ ions in MIRACLS' 1.5 keV MR-ToF device. For Doppler cooling and 300 K buffer-gas cooling the experimental (full line) as well as the simulated mass resolving power (dashed line) is shown. Fig. (b) is the same as (a) but the simulated peak-width broadening per revolution is multiplied with a factor of 3 which yields a good agreement with the experimentally obtained mass resolving power curve, see text. The revolution period t_1 is 6.62 μs.

4.2. Optimization of the mass resolving power

To optimize the mass resolving power a similar optimization procedure as described in Ref. [46] is followed. Firstly, the potentials of the four mirror electrodes constituting one MR-ToF mirror are varied in a Monte Carlo approach [31] for a fixed initial ion distribution. Secondly, the potential combinations leading to the largest R_{inf} are further optimized employing SIMION's built-in Nelder–Mead algorithm [47]. The ion injection simulation for the best mirror potentials is then optimized via the Nelder–Mead algorithm for a large transport and trapping efficiency. Finally, the in-trap lift potential is chosen such that the time for one revolution t_1 is fairly independent of the potential applied to the in-trap lift and hence the energy of the ions. Operating the MR-ToF device in this so-called isochronous mode boosts R_{inf}. The obtained potentials are stated in Table 1.

4.3. Comparison between simulations and experiment

In Fig. 2(a) the experimental and simulated mass resolving power is shown as a function of the storage time in the MR-ToF device for buffer-gas as well as Doppler cooling in the Paul trap. The measurement procedure of the mass resolving power is the same as discussed in Ref. [34]. Note that in our Doppler-cooling work only the longitudinal motion is cooled by the laser beam [34]. For comparison, an additional

simulation with 5 K buffer-gas temperature in the Paul trap is depicted. The potential tune of injection electrodes and mirror electrodes is optimized for 300 K buffer-gas cooling in the Paul trap, but also leads to very good results for 5 K buffer-gas cooling despite the difference in transversal emittance. This was confirmed by performing a dedicated potential optimization of injection and MR-ToF mirror optics for 5 K buffer-gas cooling, which yielded a similar mass resolving power as the potential tune found for 300 K buffer-gas cooling.

The initial, almost linear increase in mass resolving power can be well reproduced in simulations. It is governed by the initial peak width Δt_0, which shows an excellent agreement between simulations and experiment, see also Refs. [31,34]. For 5 K buffer-gas cooling Δt_0 is 10 ns, for Doppler cooling it is 19 ns (corresponding to 15 K buffer-gas cooling)[2] and for 300 K buffer-gas cooling it is 106 ns (measurements performed with the Paul trap settings at the time being, for possible improvements see Section 4.4). Hence, for laser cooling a mass resolving power of 100,000 can be reached within 4 ms storage time in the MR-ToF device; for 5 K buffer-gas cooling this can be achieved in 2 ms whereas for 300 K buffer-gas cooling a storage time of 22 ms is needed. The ion preparation time in the Paul trap is for buffer-gas cooling around 2 ms, whereas it is significantly increased for laser cooling to around 100 ms given the reduced buffer-gas pressure and the power density of the cooling laser. Therefore, the total processing time for mass separation of the ions is longer for laser cooling than for buffer-gas cooling for these first laser-cooling measurements [34].

Due to the peak-width broadening per revolution Δt_1, the mass resolving power approaches the maximally possible R_{inf} after some ion storage time in the MR-ToF device. For 5 K buffer-gas cooling R_{inf} is larger compared to Doppler cooling or 300 K buffer-gas cooling. This is related to the smaller longitudinal emittance which scales linearly with the ion beam temperature [48]. A reduction in longitudinal emittance results both in a reduced time as well as energy spread [34]. Due to the smaller initial time spread, a specific R value is reached faster and due to the reduced energy spread the peak-width broadening per revolution Δt_1 is decreased and R_{inf} is significantly larger compared to room-temperature buffer-gas cooling.

As visible in Fig. 2(a) there is a significant mismatch between simulated and measured mass resolving power for larger storage times. This can be corrected by multiplying the simulated peak-width broadening per revolution with the same factor of 3 for both buffer-gas and Doppler cooling, see Fig. 2(b).

Voltage instabilities of the mirror electrodes or energy fluctuations prior to the injection of the ions in the MR-ToF device can cause a reduction of the mass resolving power. In the given setup, those voltage instabilities are however much too small to explain the mismatch between experimental and simulated peak-width broadening per revolution as dedicated simulation and experimental studies show [49].

Another reason for this mismatch could be the residual gas pressure in the MR-ToF device in the experiment, whereas the MR-ToF simulations are performed assuming perfect vacuum. The importance of a good vacuum quality in the MR-ToF device has been reported repeatedly [13,14] and is observed in the present experiment as well. If more helium buffer gas is leaked into the Paul trap, the MR-ToF vacuum quality is reduced and R_{inf} is decreased. For instance, when the helium pressure in the MR-ToF device is increased from 1.2e−7 mbar to 3e−7 mbar, R_{inf} is reduced by a factor of 2.4 for the buffer-gas cooling case. Hence, the mismatch of the experimental and simulated peak-width broadening per revolution is most likely due to residual gas.[3]

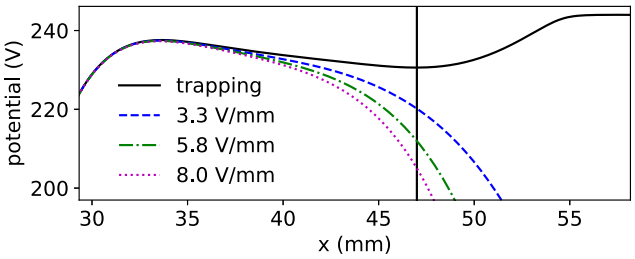

Fig. 3. Electrostatic potential along the central axis of the Paul trap of MIRACLS' low-energy MR-ToF apparatus for trapping of the ions and for three different ion extraction modes. For the latter, the potential applied to the Paul-trap's endcap is switched from 244 V during trapping to a lower value which has a strong impact on the axial field experienced by the ions. Applying 169 V, 110 V and 60 V to the extraction endcap results in field gradients at the position of the potential minimum of 3.3 V/mm, 5.8 V/mm and 8.0 V/mm, respectively. The vertical black line indicates the position of the potential minimum for trapping.

It can be concluded that the simulations are a powerful tool to find a set of MR-ToF mirror and injection potentials which allows to reach a good mass resolving power in the experiment. While the initial increase in mass resolving power is very well reproduced, the final mass resolving power R_{inf} is for both laser and buffer-gas cooling around a factor 3 overestimated in the simulations compared to experiment, which is most likely originating from the fact that collisions with residual gas particles are not taken into account in the simulations.

4.4. Operation of a 1.5 keV MR-ToF device with different Paul trap preparation schemes

For MR-ToF operation at RIB facilities with short-lived radionuclides it is important to reach a good mass resolving power in a processing time which is smaller than the nuclide's lifetime. This is a challenge for rare isotopes with halflifes on the order of a few milliseconds. Therefore the initial time spread Δt_0 needs to be as small as possible. As discussed in the previous section, laser cooling or cryogenic buffer-gas cooling lead to a much faster initial increase in mass resolving power compared to 300 K buffer-gas cooling. Nevertheless, because of its simplicity, room-temperature buffer-gas cooling is more commonly used at contemporary RIB facilities. To still reach a good mass resolving power in a short amount of time, a high extraction field strength is often applied during the Paul trap extraction [39]. The electrostatic potential along the central axis of the Paul trap in MIRACLS' low-energy apparatus is shown in Fig. 3 for ion trapping and three different extraction modes. A higher extraction field strength reduces Δt_0 at the cost of an increased energy spread of the ion bunch because of the conserved longitudinal emittance (see Fig. 14 in Ref. [34]).

As a consequence, the peak-width broadening per revolution Δt_1 and thus MR-ToF performance can be degraded if the energy spread ΔE gets too large.[4] Fig. 4(a) illustrates this interplay between Δt_0 and ΔE on the mass resolving power in our simulation studies. The Paul

[2] Note that this laser-cooling result is due to a particular combination of low-pressure buffer-gas and laser cooling as explained in Ref. [34]. Laser cooling is capable to prepare ion bunches with even smaller ToF widths and, thus, in principle, also to improve MR-ToF operation even further. The purpose of the mass resolving power measurements is to benchmark the simulations and to experimentally show that colder ion beams lead to a faster mass separation and to an increased R_{inf}. More modern MR-ToF devices exceed in R_{inf} even with conventional ion preparation, but would also benefit from colder beams for an additional boost in R_{inf}.

[3] For taking collisions between ions and residual gas particles into account in the MR-ToF simulations the knowledge of the cross sections for all ion energies in the MR-ToF device ranging from 0 to 5 keV would be required. (In our MR-ToF mirror configuration, see Table 1, ions are temporarily accelerated up to 5 keV in the refocusing sections (mirror electrode 1) of the electrostatic mirrors.) The hard-sphere interaction model which is employed for simulating the buffer-gas cooling of ions of a few electronvolts in the Paul trap may, however, not be sufficiently accurate for the present purpose and ion energy range.

[4] ΔE is in this work always given as FWHM of the energy distribution of the ions.

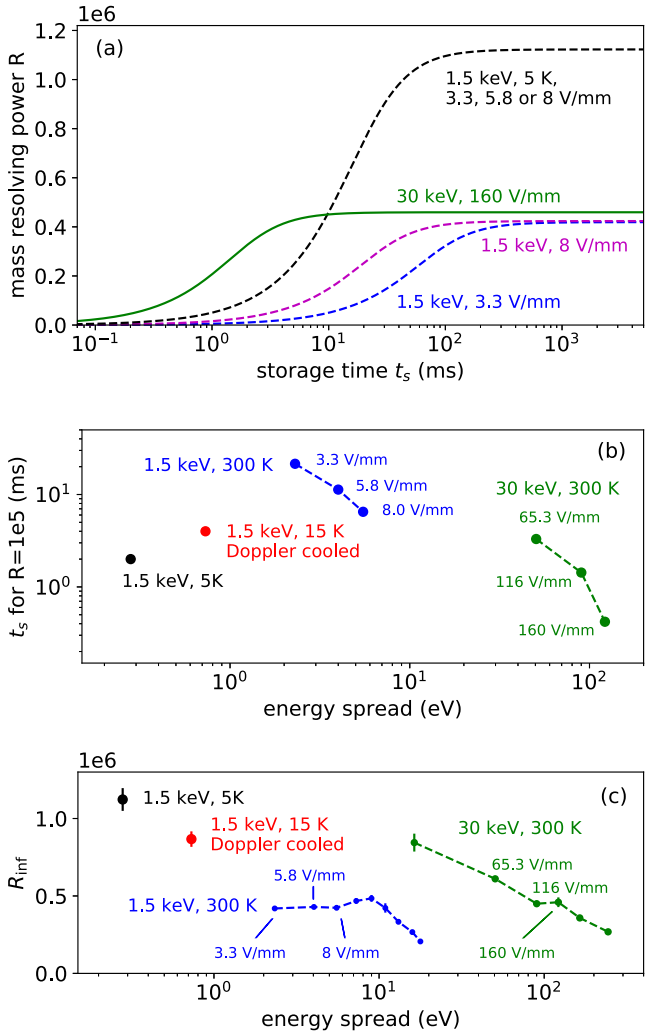

Fig. 4. Results of simulation studies for 1.5 keV and 30 keV beam energy with different Paul trap settings in MIRACLS' low-energy MR-ToF setup. (a) Mass resolving power versus storage time t_s for some selected settings. The dashed blue and dashed black curve reshow the same data as depicted in Fig. 2(a). (b) Minimum storage time t_s for reaching $R = 1e5$. Note that for determination of t_s Eq. (2) is not applicable for extraction field strengths outside the range 3–8 V/mm for 1.5 keV beam energy or 65–160 V/mm for 30 keV beam energy (see Section 4.1). (c) R_{inf} as a function of the energy spread of the ions for 1.5 keV beam energy and for 30 keV energy. For 1.5 keV beam energy the revolution period t_1 is 6.62 µs and for 30 keV beam energy it is 1.48 µs.

trap extraction scheme with a field strength of 3.3 V/mm results in $\Delta E = 2.3$ eV and $\Delta t_0 = 106$ ns and in a relatively slow increase in R over MR-ToF storage time (blue curve). For example, $R = 1e5$ is reached after 22 ms. A steeper extraction field with 8 V/mm yields $\Delta t_0 = 33$ ns and $\Delta E = 5.5$ eV (pink curve). Thus, higher mass resolving powers are obtained in a much shorter storage time. In particular, $R = 1e5$ is reached after 6.5 ms, around 3.4 times faster than for 3.3 V/mm. Note that for 5 K buffer gas cooling Δt_0 does not show any dependence on the extraction field strength as also discussed in Ref. [34]. Since for 5 K buffer gas cooling the ions are very close to the potential minimum of the Paul trap, the turn-around time [13] in longitudinal direction is minimal and Δt_0 is almost independent of the extraction field strength. When increasing the extraction field strength further to achieve even smaller storage times in the MR-ToF device for 300 K buffer-gas cooling, R_{inf} will significantly decrease (see Fig. 4(c)).

Fig. 4(b) and 4(c) show the processing time, here evaluated by the storage time t_s needed to reach $R > 1e5$, and the ultimate mass resolving power R_{inf}, respectively, for various energy spreads ΔE of the ion ensemble. Note that for the calculation of t_s from the simulations (as shown in Fig. 4(b)) the time-focus point needs to be close to the detector, while the determination of $R_{inf} = t_1/(2\Delta t_1)$ (in Fig. 4(c)) is independent of the position of the time-focus point. For room-temperature buffer-gas cooling, it is again the variation of the extraction field strength from the Paul trap which allows one to reduce Δt_0 at the cost of the increased ΔE and vice versa.

As expected, the processing time is shorter (smaller t_s) the smaller Δt_0 and, thus, the larger ΔE (see blue curve in Fig. 4(b)). Similarly, R_{inf} is increasing with decreasing ΔE (and increasing Δt_0), see blue curve in Fig. 4(c). Interestingly, this is only true above about $\Delta E \approx 9$ eV. There R_{inf} reaches a maximum below which R_{inf} is again decreasing with lower ΔE. This is interpreted as a consequence of a too low extraction field strength which has a negative impact on the transversal phase space and thus, also on the peak-width broadening per revolution Δt_1 and R_{inf}. If we artificially change the ion ensemble's energy spread while maintaining the same transversal phase space,[5] then R_{inf} keeps growing for smaller and smaller ΔE, as expected.

For comparison, Fig. 4 also shows the MR-ToF performance for ion bunches cooled via laser cooling or a cryogenic buffer gas. As discussed above, both methods allow one to obtain small Δt_0 and ΔE at the same time. Hence, a fast mass separation in combination with a large R_{inf} can be realized.

Alternatively, a fast mass separation with a high R_{inf} value may be achieved by increasing the energy-spread tolerance of MR-ToF devices while still operating the cooler-buncher at room temperature. To this end, it has been suggested that low-aberration ion mirrors may increase the energy-spread tolerances to up to 18% of the beam energy [50,51] from the current typical $\Delta E/E$ of around 1% for $R_{inf} > 1e5$. This latter value is in agreement with our simulation studies, too. To our knowledge, energy-spread tolerances of 18% have not been experimentally demonstrated so far. Alternatively, instead of increasing the relative energy-spread tolerance, the tolerance of an MR-ToF device in terms of absolute ΔE could be raised by increasing the ion-beam energy E, thus keeping the $\Delta E/E$ tolerance.

Such experiments were reported for $^{133}Cs^+$ ions stored at different ion energies within the same MR-ToF device [52]. For 1.3 keV beam energy, $R_{inf} = 4.5e5$ was reached with an energy spread of 14.3 eV while for 750 eV beam energy and an energy spread of 6 eV 'only' $R_{inf} = 2.8e5$ was obtained. Thus, the increase in beam energy from 750 eV to 1.3 keV beam energy allowed the use of a larger extraction field strength from the Paul trap which also made it possible to reach a mass resolving power of 1e5 within 2 ms[6] instead of 5 ms storage time.

4.5. Comparison of a 1.5 keV with a 30 keV MR-ToF device

Encouraged by these reports, we next explore the performance of an MR-ToF device operating at even higher ion-beam energies. Since our MIRACLS collaboration is building a 30 keV MR-ToF instrument for laser-spectroscopy applications at ISOLDE/CERN [45], the discussion will consider this specific ion energy as an example. For a direct comparison between 1.5 keV and 30 keV MR-ToF operation, simulations with a 30 keV beam energy are first performed within MIRACLS' low-energy setup as introduced in Section 3. To this end, all the MR-ToF and injection potentials are scaled up by a factor 20. Since we find a similar focal condition at the center of the MR-ToF device as for the

[5] When an ion passes the central middle plane of the MR-ToF device for the first time, the value of the total energy of this ion is exchanged with a value obtained from a Gaussian distribution. The standard deviation of the Gaussian distribution is given by the desired energy spread of the ions and the centroid is given by the average energy of all ions passing the central middle plane for the first time.

[6] In Ref. [39] a record minimum processing time of 1.7 ms is reported for reaching a mass resolving power of 1e5 for $^{133}Cs^+$ ions. The initial time spread mainly governed by the Paul-trap preparation was 9.6 ns and the energy spread was 16.9 eV.

1.5 keV case, adaptions of the injection fields are not necessary for the comparison. The Paul-trap electrodes retain their relative potential differences but are shifted by an overall floating potential. Such a scaling is presently not possible in practice due to high-voltage limitations, but the study will illustrate the advantages of high-energy MR-ToF instruments. For a realistic device, MIRACLS' dedicated 30 keV MR-ToF setup will be discussed in Section 7.

When increasing the energy of the stored $^{24}Mg^+$ ions to 30 keV within the simulated MIRACLS low-energy setup, the MR-ToF tolerance in ΔE is increased such that a fast mass separation and high R_{inf} are attainable in the same settings. As shown in Fig. 4, the 30 keV instrument exceeds the respective low-energy room-temperature simulations on both processing time and R_{inf}. When investigating different Paul-trap extraction field strengths and thus different ΔE, see Fig. 4(c), the simulation suggests that much higher R_{inf} can be reached for the higher beam energy. For an energy spread of 16 eV, for instance, R_{inf} is found to be almost twice as large in the 30 keV instrument compared to the highest R_{inf} found for an operation at 1.5 keV.

Moreover, even in the case of large extraction field strengths (e.g. 160 V/mm in Fig. 4) resulting in an energy spread as high as $\sim$ 120 eV, the obtained R_{inf} is with 4.6e5 still competitive to the highest R_{inf} achieved in the low-energy configuration. However, such an extraction leads to an initial time spread of $\Delta t_0 \approx 2$ ns obtained in the middle of the MR-ToF device which would allow one to achieve $R = 1e5$ in only 0.4 ms of storage time. Operating the MR-ToF system at this extreme necessitates the availability of a Paul trap capable to accomplish an initial time spread of less than a few nanoseconds. To our knowledge, the smallest Δt_0 reported for $^{133}Cs^+$ ions with a room-temperature Paul trap is already as short as 5 ns corresponding to an estimated energy spread of 23 eV [13], which is slightly above the tolerance in energy spread of current state-of-the-art 1.5 keV MR-ToF devices. Hence, a 30 keV MR-ToF device coupled to a room-temperature Paul trap designed for large extraction field strengths may offer a path to improved mass resolving power and to shorter processing times for MR-ToF mass separation.

5. Space-charge studies

In addition to the attainable mass resolving power and processing time, another central MR-ToF characteristic is its maximal ion flux, i.e. the number of ions which can be mass separated per unit of time. For many simultaneously trapped ions, Coulomb interactions between the ions cannot be neglected anymore. When different ion species are simultaneously trapped, these space-charge effects manifest as a confined motion of the ions inside one single bunch, which prevents any mass separation. This so-called peak coalescence effect [22,25–27] limits the ion flux.

Also below the space-charge limit where peak coalescence becomes obvious, space-charge effects can influence the ion-bunch properties of the trapped ions. Normally, the peak-width broadening per revolution Δt_1 as discussed in Section 4 leads over time to an increase in the temporal ion bunch width Δt. However, when many ions are stored in the trap Δt can stay almost constant with increasing revolution number for certain MR-ToF settings. This is referred to as selfbunching [18–25].

As both phenomena are caused by the same effect, it is meaningful to experimentally investigate the changes in Δt_1 for a single species as a first approach to study the influence of the underlying space-charge effects. In the following, the experimental method of collisional-induced fluorescence will be discussed since it allows for in-situ monitoring of the ion bunch within the MR-ToF device (Section 5.1), and the space-charge response of the system in simulation and measurement will be compared for $^{24}Mg^+$ ions (Section 5.2). Furthermore, a simulation of peak-coalescence phenomena using different ion masses will be discussed (Section 5.3).

5.1. Collision-induced fluorescence method

Collision-induced fluorescence measurements provide an excellent way to observe space-charge effects experimentally as a benchmark for MR-ToF simulations including Coulomb interactions. We explore in simulation and experiment how the ion bunch structure evolves with ion number during one storage cycle in the MR-ToF device.

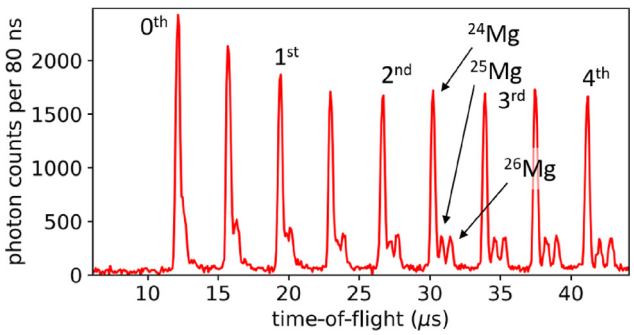

Fig. 5. Measured photon count rate versus time of flight since ion extraction from the Paul trap. The corresponding revolution numbers in the 1.5 keV MR-ToF device are indicated. The data corresponds to almost 8 million measurement cycles.

For the following measurements, the pressure in the MR-ToF device is increased to 1e−7 mbar by leaking in nitrogen through a precision needle valve installed at the vacuum chamber housing. The higher pressure increases the probability for collisions of Mg^+ ions with the gas particles. Emitted photons, following an inelastic collision, are detected by the photomultiplier tube installed above the central drift tube of the MR-ToF device. More details about the optical detection system can be found in Refs. [32,33,53,54] and in Fig. 1.

Fig. 5 shows the photon count rate as a function of the time since extraction from the Paul trap. Every time the ions pass the optical detection region in either direction in the MR-ToF device, the emitted photons can be detected. Based on this data, the peak widths corresponding to the passage of $^{24,25,26}Mg^+$ ions are extracted for every half revolution number, respectively.

Here, we extend previous, qualitative work [24] to facilitate a quantitative comparison of simulations and experiment for the ion bunch properties observed via collision-induced fluorescence. The extraction of the ion bunch shape from the simulated fluorescence signal requires precise knowledge about the detection efficiency of the emitted photons as a function of the axial position of the ions. To this end, the photon detection efficiency along the ion-beam axis of the MR-ToF device is obtained using optical ray-tracing calculations [33,53,54]. For the ray tracing, 100,000 ions are randomly displaced in transversal direction from the MR-ToF axis mimicking an ion beam of 5 mm beam diameter[7] as suggested by simulations [31]. The detection efficiency follows as the fraction of photons impinging on the PMT compared to the number of initially generated photons which are assumed to be emitted isotropically. Since only the relative photon detection efficiency as a function of the position along the ion beam axis of the MR-ToF device is relevant for the simulations, the quantum efficiency of the PMT is neglected. So it is assumed that every photon making it to the rectangular detection area of the PMT can be detected.

Fig. 6 shows the detection efficiency as a function of the position along the ion-beam axis of the MR-ToF device. The region along the ion-beam axis of the MR-ToF device, where the photon detection efficiency is large enough for efficient detection, is significantly smaller than the region that is considered to be field free.[8]

For the simulations of the photon count rate versus time-of-flight, the ion distribution is in SIMION recorded whenever the simulated 1000 ions pass the transversal middle plane of the MR-ToF device.

[7] Note that there is no relevant difference in photon detection efficiency between ion beams with diameters from 2 to 12 mm, which imposes the upper geometrical limit.

[8] The region with less than 0.04 V change in electric potential is given by -46 mm $< x <$ 46 mm [31].

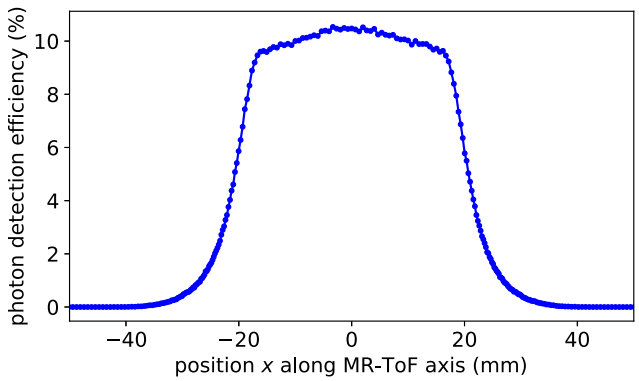

Fig. 6. Photon detection efficiency versus the position x along the 1.5 keV MR-ToF axis for 5 mm ion beam diameter. The middle plane of the MR-ToF device is at 0 mm.

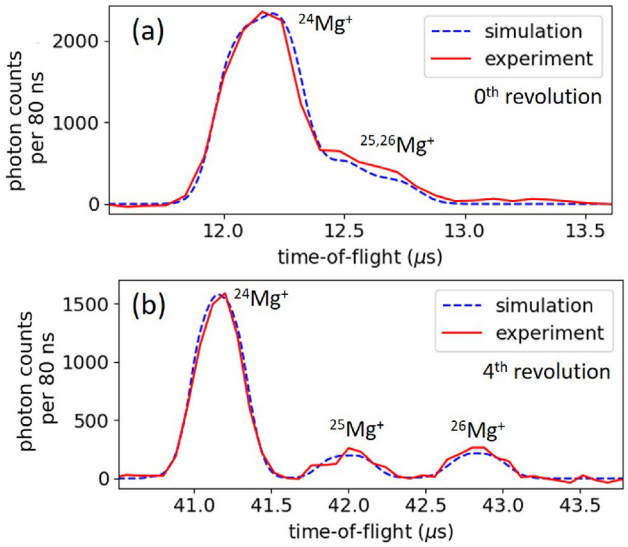

Fig. 7. Photon count rate versus time-of-flight since ion extraction from the Paul trap for $^{24,25,26}Mg^+$ ions for the very first passage through the optical detection region (a) and for the fourth revolution in the 1.5 keV MR-ToF device (b). The experimental data (red) is compared to the simulated spectrum of detected photons (blue). Space-charge effects are neglected in the simulations.

Because of the field-free region, the information of the ions' radial displacements and velocity vectors at the MR-ToF devices central plane is sufficient to calculate the entire passage through the optical detection region, which significantly speeds up the calculation time. For each chosen ion position along the ion-beam axis of the MR-ToF device the photon detection efficiency is evaluated and the detection probabilities for all ions are added up [55].

In Fig. 7 the simulated photon rate versus time of photon detection in the optical detection region is compared to experimental data for the zeroth and fourth revolution in the MR-ToF device. Since only the very first few revolutions are shown and less than 4000 ions are experimentally initially injected into the MR-ToF device (see paragraph below), space-charge effects can be safely neglected in these spectra. The simulated data are normalized in peak height to the experimental data and shifted by 330 ns, an offset in time most likely originating from HV switch delays in the experiment. Peak width and peak shape of the fluorescence signal during the ions' passage through the central drift tube are very well reproduced. This provides confidence in the validity of the simulation approach combining the ion optical simulations in SIMION with optical ray-tracing calculations of the emitted photons.

To obtain an estimate on the experimentally trapped ion number, data are recorded to count the injected ions as well as those extracted after 124 revolutions using the MagneToF detectors upstream and downstream of the MR-ToF device, respectively. These ion detectors are calibrated for ion-number determination beyond single-ion counting following a procedure discussed in Ref. [55], which is assumed to be accurate up to around 10,000 ions per bunch. When an ion bunch with a peak width on the order of 200 ns consists of more than around 10,000 ions, non-linearities of the detector response occur [55] attributed to detector dead-time effects. Based on the measurements presented in Ref. [55], it is expected that the actual ion number remains within a factor 2 the same as the experimentally determined ion number up to around 50,000 ions per bunch.

5.2. Space-charge study of ensembles of the same species

When increasing the number of simultaneously stored ions in the MR-ToF device, the peak shape and width observed in the spectrum of photons versus time can change for higher revolution numbers. For example, Fig. 8 shows the measured photon response for the 34th revolution of $^{24}Mg^+$ ions in the MR-ToF device, once for 3870(380) ions (a) and once for 18,200(1300) injected ions (b). Coulomb interactions lead to a reduction of the ToF peak width ('selfbunching') when more ions are simultaneously confined in the MR-ToF device. In both cases, the simulated photon signal is in excellent agreement with the experimental data. Between 10,000 and 20,000 ions there is no notable difference in the photon response in the simulations.

For the simulations, Coulomb interactions between the individual ions are enabled employing SIMION's built-in factor repulsion method [56]. Each particle is treated as a point charge and the particles repel each other according to Coulomb's law. For up to 1000 ions a treatment of all individual ions is computationally tractable. For a higher number of trapped ions, one ion is treated as a sub-bunch of N ions with N being the defined charge repulsion factor. E.g. to represent 1000 actual ions with 100 simulated ions, a charge repulsion factor of 10 is needed. It is important to note that only ion–ion interactions are accounted for, i.e. interactions between image charges on the electrodes and ions are not considered. Note that ion–ion interactions are only enabled within the MR-ToF device. The simulations of the ion preparation in the Paul trap and ion-beam transport to the MR-ToF device are executed without taking Coulomb interactions between individual ions into account since space charge effects in the Paul trap for up to 50,000 injected ions into the MR-ToF device are almost negligible for the MR-ToF performance as dedicated simulation studies have shown.

5.2.1. Comparison between simulations and experiment

In order to benchmark the space-charge simulation code more comprehensively, collision-induced fluorescence measurements are performed for up to 124 revolutions utilizing different in-trap lift potentials as well as different numbers of injected ions into the MR-ToF device. When increasing the in-trap lift potential U_{lift}, the kinetic energy of the stored ions reduces linearly, $E_{\mathrm{trapped}} = E_{\mathrm{injected}} - U_{\mathrm{lift}}$. This allows one to operate the MR-ToF device either in dispersive, selfbunching or isochronous mode [24,25]. The peak widths of the measured and simulated photon response to the $^{24}Mg^+$ ion passage is shown in Fig. 9 as a function of revolution number for three different in-trap lift potentials and different ion numbers.

For an in-trap lift potential of 850 V, the MR-ToF device is operated in isochronous mode, in which the revolution period t_1 is fairly independent of the energy E of the individual ions, hence $dt_1/dE \approx 0$. The peak width over revolution number remains constant in this mode, irrespective of the number of confined ions, see Fig. 9(a,b). For ion numbers exceeding 20,000 ions a slight increase of the peak width is visible in both simulations as well as experimental data, which indicates that it is more difficult to maintain an isochronous mode when more ions are simultaneously stored.

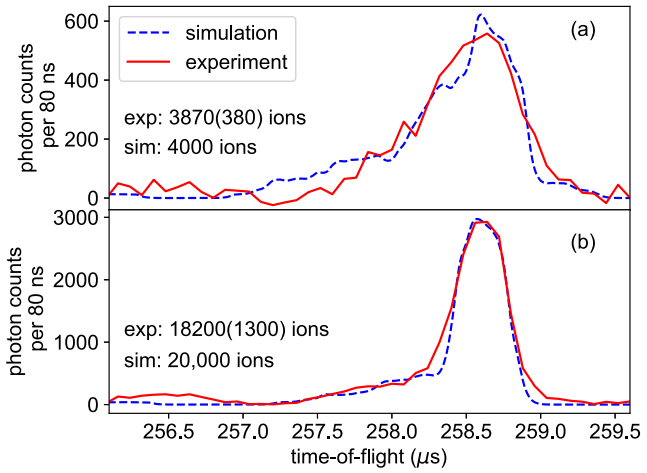

Fig. 8. Photon counts versus time-of-flight since ion extraction from the Paul trap for $^{24}Mg^{+}$ ions for the 34th revolution and an in-trap lift potential of 700 V in MIRACLS' low-energy MR-ToF device. The experimental data (red) is compared to the simulated ToF spectrum of detected photons (blue). For (b) the ion number is around a factor 5 larger than for (a).

If an in-trap lift potential of 995 V is chosen, the MR-ToF device is operated in dispersive mode with $dt_1/dE < 0$. In this mode, the peak width increases over revolution number, see Fig. 9(c) and for a higher number of stored ions the bunch disperses faster, see Fig. 9(d). Note that only 400(100) of the initially 8740(520) injected ions can be extracted after 124 revolutions. The low storage efficiency in the MR-ToF device is a consequence of the vacuum pressure of 1e−7 mbar needed to increase the collision probability in order to obtain enough statistics within a few days of measurements. However, this also implies that more and more ions are lost due to ion-gas collisions the longer the ions are confined in the MR-ToF device. In the simulations assuming perfect vacuum, the storage efficiency is more than 90% irrespective of the number of simultaneously confined ions as tested for up to 25,000 ions. These 10% losses take place in the simulations during the first few revolutions only.

For an in-trap lift potential of 700 V, the relation $dt_1/dE > 0$ holds and the ion bunch is also dispersing (Fig. 9(e)). However, if the charge density of stored ions is high enough, Coulomb interactions lead to the self-bunching effect and the peak width stays fairly constant over revolution number (Fig. 9(f)). This self-bunching phenomenon is well reproduced by the simulations. For lower numbers of stored ions in this configuration, there is a small difference between simulation and experiment, see again Fig. 9(e). Among all cases studied, $U_{\text{lift}} = 700$ V with an intermediate ion number shows by far the strongest dependence of the peak-width broadening per revolution on the exact ion number, see simulation results in Fig. 9(e). Thus, any smaller sized inaccuracies in ion number, either in the measured ion number, intensity fluctuations or ion losses, may lead to more notable shifts in this particular configuration.

Generally, for around 20,000 injected ions the experimental peak widths are slightly larger than predicted by the simulations (see Fig. 9(b,f)). This effect was studied in Refs. [57,58] and was attributed to the Coulomb repulsion in the Paul trap, which is neglected in the present simulations to keep the simulation times reasonably short.

Overall, the comparison of the simulations with experimental data with ions of the same species provides confidence in the space-charge simulations. The simulations with up to 25,000 simultaneously stored ions show a good qualitative agreement with experimental data. The charge repulsion factor method in SIMION provides a powerful tool for our purposes (for a charge repulsion factor up to at least 250, see Appendix) while reducing the simulation time significantly. Given the good agreement between the SIMION simulations and our experimental data, we consider SIMION as an appropriate tool to estimate the onset of space-charge effects in MR-ToF devices. Thus, it can provide a qualitative guidance to reduce space-charge effects in MR-ToF systems.

5.3. Study of the interaction of two ensembles of different ion species

After benchmarking the space-charge simulation code with experimental data for one ion species trapped in the MR-ToF device, it will in the following be used to investigate the peak coalescence effect in dedicated simulations. To this end, ions of hypothetical masses 24 u and 24.0096 u ($m_1/(m_2-m_1) = 2500$) and an abundance ratio (see Section 2 for a definition) of $r_{\text{ab}} = 9$ are thermalized with 300 K buffer gas in the Paul trap, transported to the MR-ToF device and stored simultaneously for 150 revolutions at a beam energy of 1.5 keV. Fig. 10 shows the simulated time-of-flight spectra of the ions after 150 revolutions as recorded at the middle plane of the MR-ToF device. For up to around 3000 stored ions the two ion species are well separated in time-of-flight after 150 revolutions. Starting from 5000 ions more than 7% of the ions of mass 24 u are overlapping in time-of-flight with ions of mass 24.0096 u and hence cannot be fully mass separated anymore. For 25,000 ions a full peak coalescence is observed. However, some ions lose synchronicity with the main ion bunch (see Fig. 10(f)). When the ion number is further increased less ions lose synchronicity (not shown). The dependence on mass, the $m_1/(m_2-m_1)$ ratio and the abundance ratio, will be discussed in the following sections, see e.g. Figs. 12 and 16.

The peak coalescence simulations presented in this work show a good agreement with earlier simulations performed in Simbuca [59] and experimental data from the same MR-ToF device, while it had been operated earlier at Greifswald [26,27]. For those simulations the ion distribution was initialized directly in the axial center of the MR-ToF device. The present work goes a step further, and the full process from thermalization in the Paul trap up to ion storage in the MR-ToF device is simulated. This comprehensive approach is required to predict and optimize the ion flux, i.e. the number of ions which are mass separated and transmitted per unit time. In the following this is investigated for various experimental conditions including different schemes in the ion preparation prior to the ion storage in the MR-ToF device itself.

6. Ion flux simulations

6.1. Ion flux for ion doublets with $m_1/(m_2 - m_1) = 2500$

In this section, the maximal ion flux is evaluated for different Paul trap and MR-ToF operation modes for a storage time leading to a mass resolving power of 5000. The $m_1/(m_2-m_1)$ ratio of the two ion species to mass separate is chosen with 2500 in order to fully mass separate them in the limit of single ion counting [12]. The two ion species have mass $m_1 = 24$ u and $m_2 = 24.0096$ u, respectively, and an abundance ratio $r_{\text{ab}} = 9$. While $R = 5000$ is a very modest mass resolving power for which next-generation magnetic separators outperform MR-ToF devices in ion flux, it is chosen for the simulations in this section as it is still fully tractable.[9] It allows conclusions about the effects caused by high ion flux in MR-ToF devices at low R and low mass which are confirmed to be valid also for the experimentally more relevant larger R and ion masses, as discussed in Section 6.2.

The maximal ion flux is in the following defined by N_{max}/t_s, so it is limited by the storage time t_s in the MR-ToF device as well as by the maximal ion number N_{max} that can be confined simultaneously in the MR-ToF device without notable peak overlap due to the peak

[9] Due to limitations in computing resources, only a few hundred revolutions can be simulated with sufficient accuracy and reasonable run times. Hence, most of the simulations discussed in the following are limited to a storage time of 1 ms (corresponding to up to 150 revolutions for $^{24}Mg^{+}$ ions with 1.5 keV beam energy).

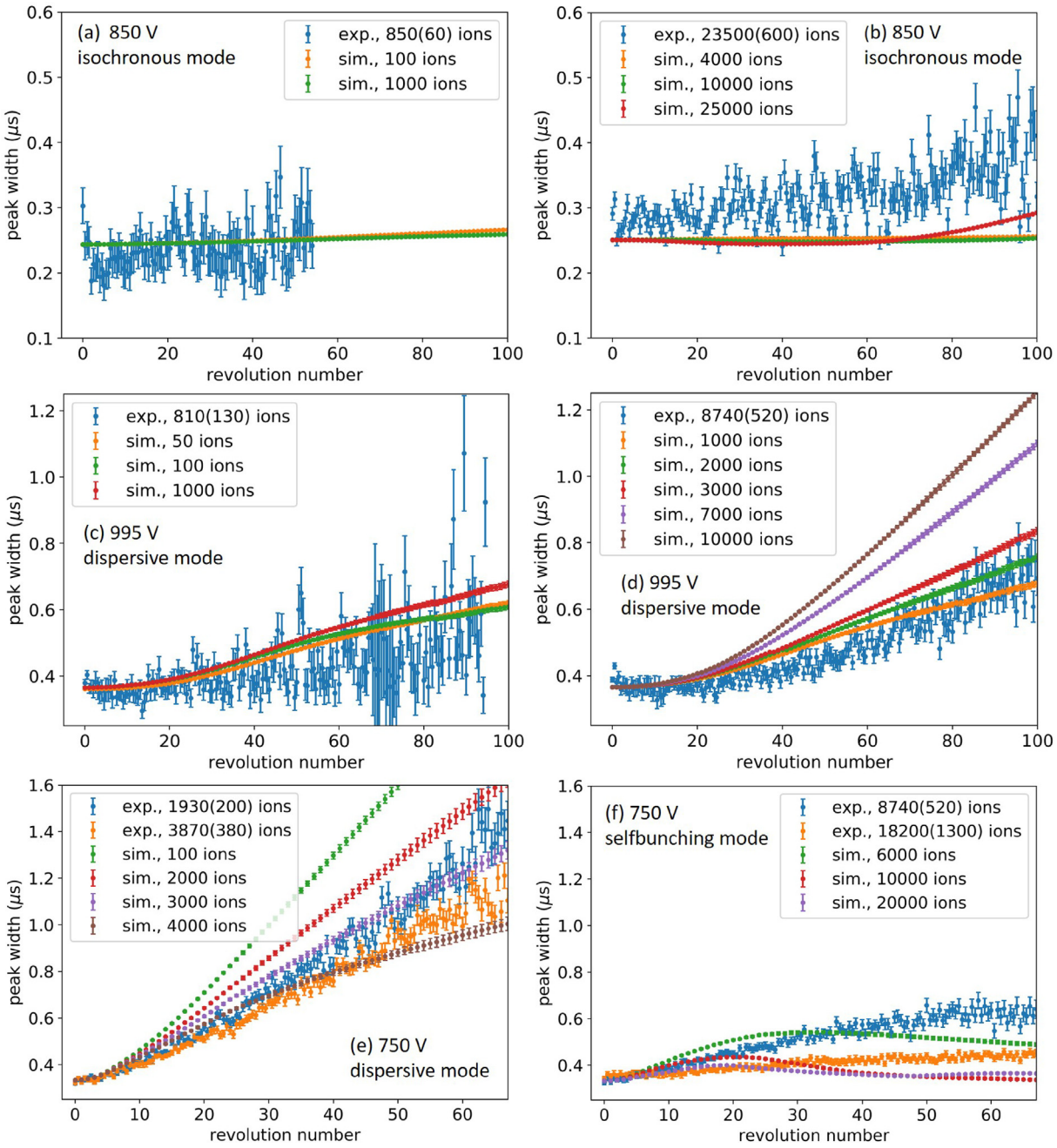

Fig. 9. Simulated and measured peak widths of the photon signal during ion passage versus revolution number for different numbers of injected ions and MR-ToF in-trap lift potentials of the 1.5 keV MR-ToF device. The left column shows scenarios with a smaller number of simultaneously stored ions than the right column. Note that measurements and simulations as shown in (a) and (b) are performed with an accidentally 25-degree rotated slit in front of the PMT. While this has no overall impact on the plotted comparisons and conclusions, it explains the slightly smaller peak width for 0 revolutions in (a,b) compared to (c–f). For higher revolution numbers than shown it is not feasible to extract the peak widths due to too little statistics.

coalescence effect. Note that a more general definition of the ion flux is given in Section 2 (see Eq. (1)), where the ion flux is defined by $N_{\mathrm{max}}/t_{\mathrm{proc}}$. As the present work aims to characterize the behavior of the MR-ToF mass separator itself, the processing time t_{proc} is equated with the storage time t_s.

In the case of a 300 K buffer gas and a field strength of 3.3 V/mm in the Paul trap $R = 5000$ can be reached in MIRACLS low-energy device for 24 u ions within a storage time t_s of 1 ms. For a higher extraction field strength with either 8 V/mm or 10.6 V/mm or alternatively a reduced buffer-gas temperature, less storage time is needed to achieve the same mass resolving power due to the reduced initial time spread as already discussed in Section 4.1. The initial time spread Δt_0 and the storage time t_s, after which $R = 5000$ is reached, are shown in Figs. 11(a,b) for different extraction field strengths and buffer-gas temperatures, respectively.

The maximum number of stored ions N_{max}, before more than 7% of the two ion species are overlapping in time-of-flight due to peak coalescence, is shown in Fig. 11(c) for the different Paul trap settings.[10] The simulations reveal that for a smaller initial time spread fewer ions can be simultaneously stored in the MR-ToF device. This is interpreted

[10] The top of the error bar indicates the ion number for which more than 7% of the ions are overlapping while the bottom of the error bar marks the ion number where the overlap is less than 7%. The same applies for all other ion flux figures.

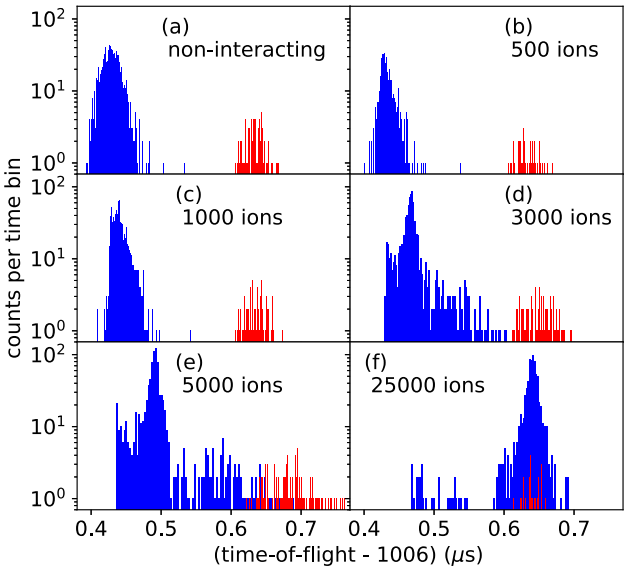

Fig. 10. Simulated time-of-flight spectra of ions with mass 24 u and with mass 24.0096 u simultaneously stored in the 1.5 keV MR-ToF device after 150 revolutions. In (b) 450 ions with 24 u and 50 ions with 24.0096 u are simulated and in all other cases 900 ions with 24 u and 100 ions with 24.0096 u are simulated. In (b,c) a charge repulsion factor of 1 is used, in (d) a factor of 3, in (e) a factor of 5 and in (f) a factor of 25. 300 K buffer-gas cooling is employed and the extraction field strength in the Paul trap is 8 V/mm.

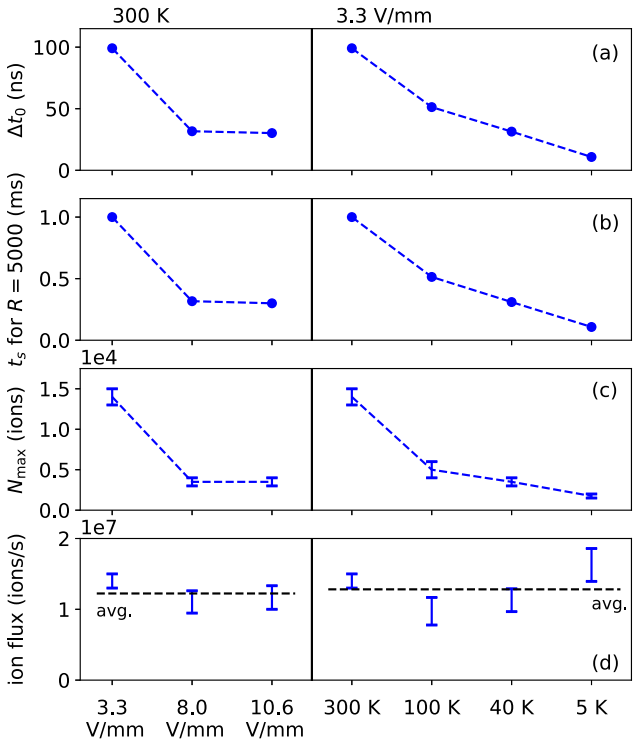

Fig. 11. (a) Initial time spread Δt_0 recorded when the ions pass the middle plane of the 1.5 keV MR-ToF device the first time for different Paul-trap preparation settings. The first three data points are performed for 300 K beam temperature and 3 different extraction field strengths, the last 4 data points are for an extraction field strength of 3.3 V/mm and different buffer gas temperatures. (b) Necessary storage time t_s to reach the mass resolving power $R = 5000$ for the different settings. Error bars in (a) and (b) are smaller than the dots. (c) Maximal number N_{max} of simultaneously stored ions before more than 7% of the ions are overlapping due to the peak coalescence effect for the different settings. (d) The maximal ion flux, given by N_{max}/t_s versus the different Paul-trap preparation settings. The average is indicated by a dashed horizontal line. The simulations are performed with ions of mass 24 u and 24.0096 u ($m_1/(m_2-m_1) = 2500$) with an abundance ratio $r_{ab} = 9$. Charge repulsion factors of up to 17 are used to simulate up to 17,000 simultaneously stored ions in the MR-ToF device.

as a consequence of ions being closer together in time-of-flight and thus also in space in longitudinal direction such that the ions will experience stronger Coulomb interactions, especially effective during their velocity reversal in the mirror electrodes.

The resulting maximal ion flux N_{max}/t_s, is shown in Fig. 11(d) for the different investigated cases. Even though a given R is reached more quickly for a smaller initial time spread Δt_0, the ion flux remains within statistics the same. For a smaller Δt_0 fewer ions can be stored simultaneously in the MR-ToF device due to the earlier onset of peak coalescence. Thus, as long as the half-lives of investigated nuclides are long enough to allow a mass separation within the necessary storage time, our simulations suggest that there is no notable advantage for an MR-ToF device's maximal ion flux using a Paul trap capable to obtain a small initial time spread Δt_0. If the ion bunch preparation time t_{prep} in the Paul trap is not neglected and one operates with settings $t_s < t_{prep}$, a faster mass separation (hence smaller Δt_0) leads to a reduction of the ion flux defined via $N_{max}/\max(t_s, t_{prep})$ since for smaller Δt_0 less ions can be simultaneously confined in the MR-ToF device.

Experimental ion flux measurements were carried out in earlier work utilizing the same MIRACLS 1.5 keV MR-ToF device for $A = 28$ [26,27]. These experimental studies showed that for 1.5e7 ions/s a separation of N_2^+ and CO^+ ions ($m_1/(m_2 - m_1) = 2500$) is possible, whereas for 6.25e7 ions/s a significant peak coalescence prevents the mass separation. The experimentally determined maximal ion flux is hence very close to the one simulated in this work, providing further confidence in our simulation approach (see inset of Fig. 12).

6.2. Ion flux for larger $m_1/(m_2 - m_1)$ ratios

While the previous simulations illustrated that the ion preparation has no significant impact on the ion flux as long as $t_s > t_{prep}$, we discuss next the relationship between maximal ion flux and $m_1/(m_2 - m_1)$ ratio of the ion species to be mass separated. In particular, one needs to take into account that for ions closer in mass the maximal attainable ion flux significantly drops. Fig. 12 shows the maximal ion flux versus $m_1/(m_2 - m_1)$ of the present simulation work for MIRACLS' 1.5 keV MR-ToF device for $A = 24$ (blue data points) compared to other experimental and/or simulation studies (gray data points). Due to too long simulation run times, we cannot easily extend our simulations in the 'standard' Paul trap operation to $m_1/(m_2 - m_1) > 5000$. For larger $m_1/(m_2 - m_1)$, we thus perform simulations with 5 K buffer-gas cooling. This reduces t_s to a tractable value while the maximal ion flux is comparable with the room-temperature case (see Fig. 11).

The ion flux simulations for the ORISS MR-ToF device planned for FRIB [60] are performed with Warp [64], an open-source particle-in-cell Python package. The simulations are carried out for $A = 238$ and $m_1/(m_2 - m_1) = 238$, thus, separating ions with 238 u from contaminants with 239 u. They show a reasonably good agreement with the ion flux simulations from the present work.

As mentioned in Section 6.1, the measured maximal ion flux for MIRACLS' low-energy MR-ToF device [26,27] agrees with simulation studies in Simbuca [59] as well as with the present work (see inset of Fig. 12 and discussion in Section 6.1).

Also the experimentally reported maximal ion flux values for ISOLTRAP [61], TITAN [14,62,63] and Giessen MR-ToF devices [13] with different $m_1/(m_2 - m_1)$ are in line with the simulations performed in this work. Note that at TITAN, a two-step strategy is adapted in which at first MR-ToF mass separation of 1e6 to 1e7 ions/s with $m_1/(m_2 - m_1) < 1e4$ is performed followed by a mass selective retrapping in the Paul trap to remove a large fraction of the contaminants. Finally, a high-precision mass measurement of the remaining 50 ions/s with up to $m_1/(m_2 - m_1) = 2.5e5$ is conducted in the MR-ToF device [14,62,63].

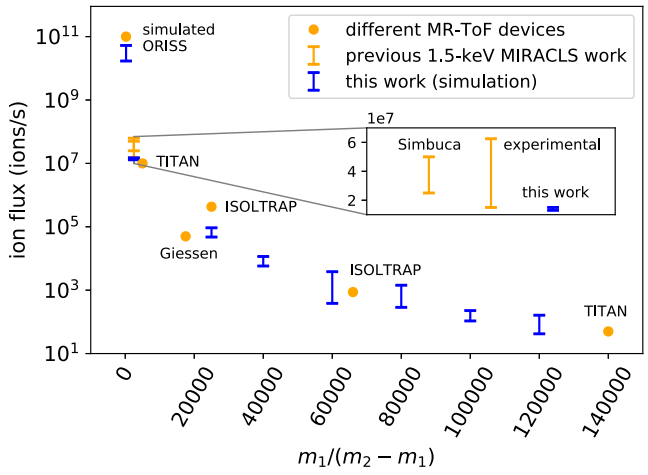

Fig. 12. Maximal ion flux versus $m_1/(m_2-m_1)$ for different low-energy MR-ToF devices (orange). The simulations for the ORISS MR-ToF device are performed for $A = 238$ [60]. The ion flux measurements from ISOLTRAP are for $A = 152$ [61], from Giessen for $A = 78$ [13], and from TITAN for $A = 28, 60, 131$ and 151 [14,62,63]. The simulated ion flux values for MIRACLS' 1.5 keV MR-ToF device for $A = 24$ are shown in comparison (blue). For $m_1/(m_2-m_1) = 2500$ also simulations in Simbuca [59] were performed for the MIRACLS 1.5 keV MR-ToF device for $A = 28$ as well as dedicated measurements [26,27] (see inset). All values above or equal $m_1/(m_2-m_1)$=1e5 are resulting from only confining one single ion in the MR-ToF device.
Additional information: The reported ion flux values for TITAN are the limit for high-precision mass measurements, the ones for mass separation are expected to be slightly larger. For ISOLTRAP's ion flux measurements more than 7% of the ions are overlapping, especially for $m_1/(m_2-m_1) = 27{,}200$, which is most likely explaining its offset from our simulations and the ion flux reported from Giessen.

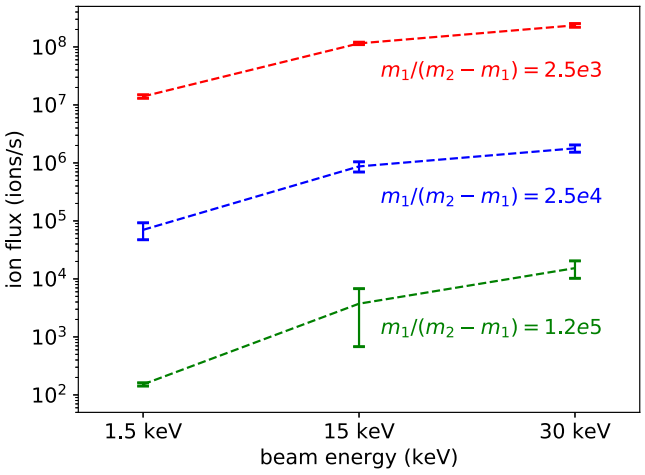

Fig. 13. Maximal attainable ion flux for different beam energies and mass differences in MIRACLS' low-energy MR-ToF setup. For 1.5 keV beam energy the simulations are performed with an extraction field strength of 3.3 V/mm, for 15 keV beam energy with 33 V/mm and for 30 keV beam energy with 65.3 V/mm. Simulations with $m_1/(m_2-m_1) = 2500$ are performed with mass 24 u and 24.0096 u, simulations with $m_1/(m_2-m_1) = 25{,}000$ with 24 u and 24.00096 u and simulations with $m_1/(m_2-m_1) = 1.2e5$ are performed with 24 u and 24.0002 u. The abundance ratio is always 9. Charge repulsion factors of up to 80 are used to simulate up to 40,000 simultaneously stored ions.

The overall good agreement with existing measurement data as well as other simulation codes provides additional confidence in the present simulation approach. Interestingly, the maximal ion flux seems to be within a factor of 4 fairly independent of the different MR-ToF designs, different masses ranging from $A = 24$ to $A = 238$ and different abundance ratios between ions of interest and contaminants. For a more detailed discussion on the influence of mass and abundance ratios on the maximal ion flux see Section 7.3.

6.3. Boosting the ion flux with a higher-energy MR-ToF device

For many applications at RIB facilities it is required to be able to provide isobarically pure beams with higher ion flux. For this purpose, one may consider to perform the mass separation very fast and only have maximally one ion stored in the MR-ToF device at a given time. In practice, such an approach will face a technical limit either by the involved electronics or the ion preparation in the Paul trap. As an alternative path, one may identify an MR-ToF configuration allowing to store more ions simultaneously in the MR-ToF device without significant space-charge effects.

As we have shown above, due to its larger tolerance in energy spread a 30 keV MR-ToF device can be advantageous for a faster mass separation of isobars. As another, possibly even more important benefit, our simulations indicate that the ion-flux can be significantly boosted when increasing the MR-ToF ion-beam energy. To this end all the potentials in the MIRACLS low-energy setup are scaled up in the simulations to allow ion storage in the MR-ToF device with either 15 keV or 30 keV in analogy to the discussion in Section 4.4. Fig. 13 summarizes the results in terms of maximal ion flux for 1.5 keV, 15 keV and 30 keV beam energies. In all cases, the abundance ratio between ions of interest and contaminants is 9.

For 1.5 keV beam energy, 5 K buffer-gas temperature and $m_1/(m_2-m_1) = 1.2e5$, space-charge effects become dominant as soon as only a few ions are simultaneously stored in the MR-ToF device. Thus, the maximal ion flux is simply calculated by $1/t_s$ with a storage time t_s of 6.2 ms necessary to reach $R = 2.4e5$. For 15 keV beam energy, 5 K buffer-gas temperature and $m_1/(m_2-m_1) = 1.2e5$ peak coalescence is observed for 10 interacting ions (upper limit in Fig. 13). The lower ion flux limit is given by storing only one ion at a time in the MR-ToF device. For 30 keV beam energy, 5 K buffer gas temperature and $m_1/(m_2-m_1) = 1.2e5$, no peak coalescence is visible for 10 interacting ions (lower limit), but for 20 interacting ions effects towards peak-coalescence become visible (upper limit in Fig. 13).

Confirming our previous conclusion once more, configurations which only differ in their ion preparation yield a similar maximal ion flux (not shown). When comparing the ion flux simulations for the three different beam energies however, it becomes apparent that a factor 6 to 12 higher maximal ion flux is achieved when increasing the beam energy from 1.5 keV to 15 keV. At 30 keV the increase is even a factor of 13 to 25. Hence, our simulations suggest that an increase in beam energy of the stored ions will allow to reach a significantly higher ion flux. This can be attributed to the observation that for the same temporal ion bunch width Δt a 30 keV ion beam is further spatially spread in longitudinal direction compared to a 15 keV or 1.5 keV ion beam.

7. A 30 keV MR-ToF mass separator

7.1. Conceptual design and operational parameters

A dedicated 30 keV MR-ToF system is currently in development at ISOLDE/CERN for the purpose of highly sensitive, high-resolution collinear laser spectroscopy at MIRACLS [45]. Reflecting its potential for highly selective mass separation, we propose an MR-ToF system by reconfiguring the components of MIRACLS' 30 keV apparatus for improved mass separation. Its performance is studied in simulations to guide experimental work on a future ISOLDE MR-ToF mass separator. An overview of the proposed setup is shown in Fig. 14. The radioactive ion beam produced at ISOLDE is injected into MIRACLS' linear room-temperature buffer-gas filled Paul trap, which is floated to 50 kV. After the ions are extracted as bunches from the Paul trap with an extraction field strength of around 14 V/mm, they are accelerated to a kinetic energy of 2 keV. They pass two einzel lenses (L1 and L2) before they

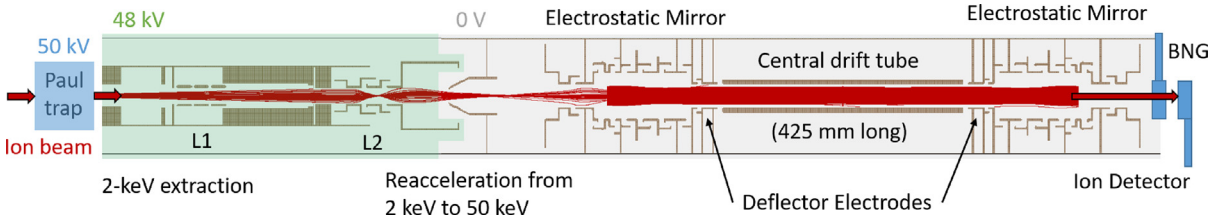

Fig. 14. Proposed 30 keV MR-ToF mass separator system: Cut view of its electrode structure together with the ions' trajectories in red for 100 ions performing 100 revolutions (the electrode structures are to scale, the housing vacuum chambers are simplified). Additionally, the Paul trap for preparation of the ion bunches upstream of the MR-ToF setup and the potential location of a (retractable) BNG and detector system downstream of the MR-ToF device are schematically shown (not to scale). The full system takes up a floor space of around 1 m × 3 m.

are reaccelerated to 50 keV at the entrance of the MR-ToF device. By switching the in-trap lift from around 20 kV to ground potential the ions are stored in the MR-ToF device at around 30 keV beam energy until the necessary mass resolving power is reached.

The removal of the time-of-flight mass separated contaminants is either possible by dedicated deflector electrodes installed between the central drift tube and the MR-ToF mirrors during the ions storage time in the MR-ToF device [65], by mass-selective ion ejection via a pulsed in-trap lift [66] or by a Bradbury–Nielsen-Gate [67] installed downstream of the MR-ToF device, possibly after a dedicated deceleration region for a reduction of the beam energy from 50 keV down to a few kiloelectronvolts. A retractable ion detector downstream of the Bradbury–Nielsen-Gate (BNG) allows time-of-flight measurements of the extracted ions as well as beam diagnostics. When retracting the ion detector the purified ion beam can be transported to the dedicated experimental setups.

The transfer beam line between Paul trap and reacceleration region is floated to 48 kV, whereas the beam line housing the 30 keV MR-ToF device is grounded.

The distance between Paul trap and MR-ToF device should be as short as possible such that the time-focus point can be matched onto a detector/BNG plane installed directly downstream of the MR-ToF device for large extraction field strengths from the Paul trap. This enables a fast mass separation as beneficial for radionuclides with very short half-lives. Since there needs to be space for two einzel lenses and a reacceleration region which also serves as a differential pumping barrier, a Paul-trap operation with initial time spreads below 16 ns will not allow to match the time-focus point at the detector plane. As discussed in previous sections, a fast mass separation will for most applications not boost the ion flux. Hence, initial time spreads of around 16 ns are sufficient.

The 30 keV MR-ToF device itself is based on MIRACLS' instrument as designed for high-resolution collinear laser spectroscopy [45]. The potential combination of the MR-ToF mirror electrodes as optimized for collinear laser spectroscopy also leads to a reasonably large mass resolving power, once the length of the central drift tube is properly chosen. The standard optimization procedure to obtain suitable injection and MR-ToF mirror potentials (see Section 4.2), did not reveal a configuration with significant improved performance in mass separation. The highest mass resolving power R_{inf} is achieved for a length of the central drift tube corresponding to 425 mm, a potential of −1.6 kV applied to lens 1 and −18.1 kV applied to lens 2 with respect to the 48 kV potential of the transfer beam line. The in-trap lift potential is found to be optimal at 18.79 kV. For this in-trap lift potential the setup is operated in isochronous mode, hence the revolution period is fairly independent of the energy of the individual ions. All other operational settings and geometries are identical to the ones stated in Ref. [45].

7.2. Mass resolving power

The simulated total transport and storage efficiency from extraction from the Paul trap, ion transfer and ion storage in the MR-ToF device is found to be 91%. The simulated mass resolving power for the new 30 keV MR-ToF system for $^{24}Mg^{+}$ ions is shown in Fig. 15 as a function of storage time in comparison to the simulated mass resolving power for MIRACLS' 1.5 keV MR-ToF setup, for 300 K buffer-gas cooling as well as for hypothetical 5 K buffer-gas cooling. In the proposed setup, the simulations predict a mass resolving power of 1e5 after a storage time of 3 ms, corresponding to 750 revolutions in the MR-ToF device. The maximal achievable mass resolving power R_{inf} is 1.15e6. Note that in practice the experimentally achievable mass resolving power is expected to be lower due to the non-ideal vacuum pressure and voltage fluctuations. As discussed in Section 4.3 for MIRACLS' 1.5 keV system, the reduction from simulated to experimental R_{inf} is a factor 3. It is assumed that the impact of the residual gas pressure on R_{inf} will be less severe for the 30 keV MR-Tof device since the vacuum quality in the new 30 keV device will be improved compared to the one in MIRACLS' low-energy apparatus, e.g. by proper differential pumping to prevent He gas from the Paul trap to reach the MR-ToF device.

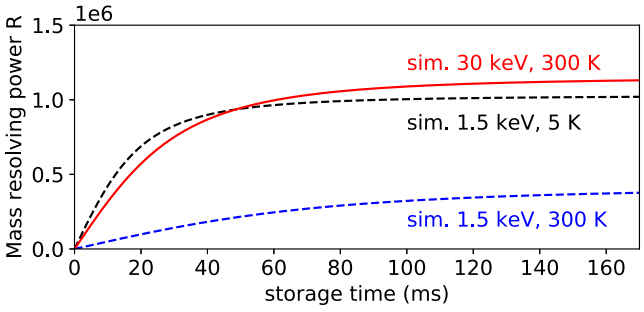

Fig. 15. Simulated mass resolving power versus storage time of MIRACLS' new 30 keV mass separator (full line) in comparison to the simulations performed in MIRACLS' low-energy MR-ToF setup (dashed lines) for $^{24}Mg^{+}$ ions. In the MIRACLS low-energy setup the revolution period is 6.62 μs for 1.5 keV beam energy and in the new 30 keV setup it is 4.00 μs.

7.3. Ion flux

Fig. 16 shows the simulated maximal ion flux in the proposed 30 keV MR-ToF system for different masses, abundance ratios and in-trap lift potentials. The ratio $m_1/(m_2 - m_1)$ is 25,000 for all cases investigated to achieve a mass separation within less than 500 revolutions. The necessary storage time for $R = 50{,}000$, in which a full mass separation of non-interacting ions is possible, is 1.52 ms for $A = 24$, 3 ms for $A = 132$ and 4.7 ms for $A = 250$. For almost all simulations there is hardly any dependence of the maximal ion flux on the abundance ratio (see Fig. 16(a) for $A = 24$ and 18790 V applied to the in-trap lift). Only the simulations with abundance ratios of 9 or 49 show a factor 2–4 loss of ion-flux capabilities. For those the less abundant mass (e.g. 24.00096 u) starts for a higher number of stored ions to be hidden in the tail of the more abundant mass (e.g. 24 u). The tail in the ToF spectrum towards higher ToF values is attributed to

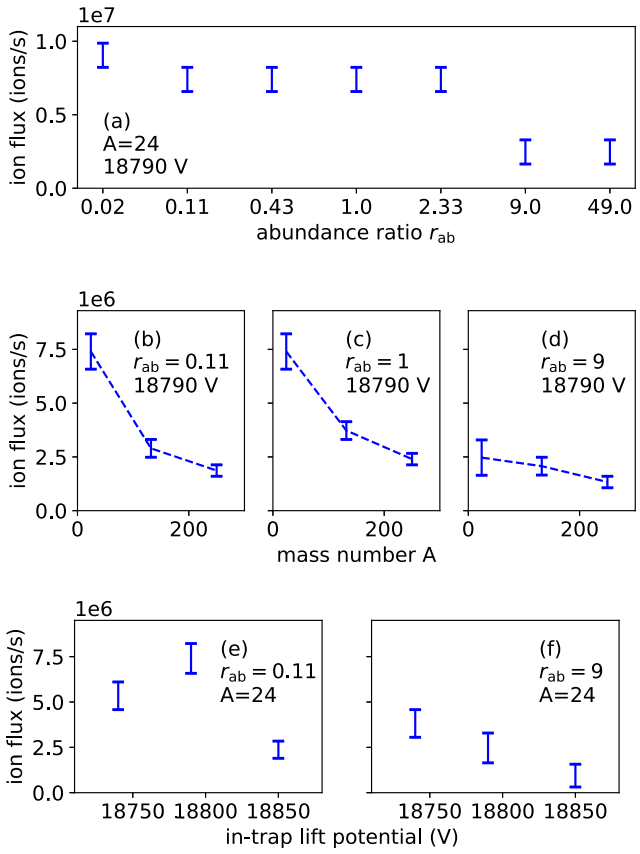

Fig. 16. Maximal ion flux for $m_1/(m_2-m_1)=25{,}000$ in the new 30 keV MR-ToF mass separator for different masses, abundance ratios and in-trap lift potentials. (a) Maximal ion flux as a function of the abundance ratio for $A=24$ and 18790 V applied to the in-trap lift (isochronous mode). (b–d) Maximal ion flux as a function of the mass number A of the ions for three different abundance ratios and isochronous operation. (e,f) Maximal ion flux as a function of the in-trap lift potential. For 18740 V applied to the in-trap lift the device is operated in selfbunching mode, for 18790 V in isochronous mode and for 18850 V in dispersive mode. In total always 500 ions are simulated with different charge repulsion factors up to 30, to simulate up to 15,000 simultaneously stored ions.

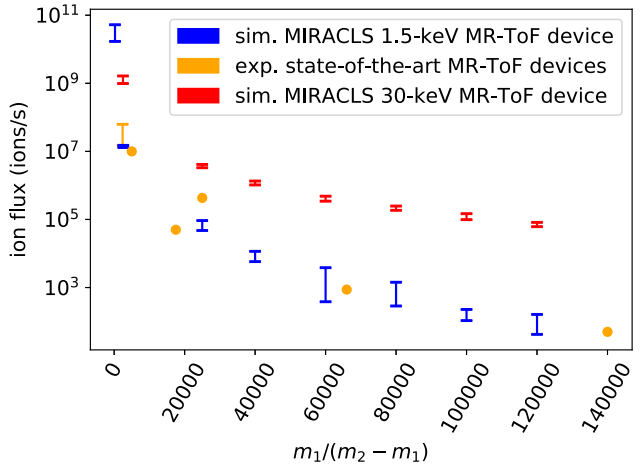

Fig. 17. Maximal ion flux versus $m_1/(m_2-m_1)$ for MIRACLS' 1.5 keV MR-ToF device (simulation), different low-energy MR-ToF devices (experiment) and MIRACLS' new 30 keV MR-ToF mass separator (simulation). The black and orange data are the same as shown in Fig. 12. The simulations for MIRACLS' 30 keV MR-ToF device are performed for $A=132$ and a charge repulsion factor smaller than 30, except for $m_1/(m_2-m_1)=2500$ where it is 500 in order to simulate 250,000 interacting ions. As of computational limitations, the number of sample ions used for $R>80{,}000$ is decreased from 500 to 300 ions.

reheating effects in the Paul trap due to buffer gas collisions during ion beam extraction [49].[11]

When increasing the mass to $A=250$, the maximal ion flux drops by a factor 2–4 for all three abundance ratios studied (see Figs. 16(b-d) for an in-trap lift potential of 18790 V). Thus, the ion flux is only very slightly dependent on mass or studied abundance ratio. The maximal ion flux however shows some dependence on the in-trap lift potentials (see Figs. 16(e,f) for $A=24$ and two different abundance ratios). Slight selfbunching (18740 V applied to the in-trap lift) can be beneficial in specific cases compared to isochronous operation (18790 V) or especially the dispersive region (18850 V).

The achievable ion flux of around 7e6 ions/s for $A=24$ and $m_1/(m_2-m_1)=25{,}000$ is around a factor 70 larger compared to the MIRACLS' low-energy device. A factor of around 20 can be explained by the increase in ion-beam energy from 1.5 to 30 keV, see Section 6.3. The remaining factor ≈3.5 is attributed to changes in the MR-ToF design.

Based on the studies in Section 6.3, a similar improvement can be expected for higher $m_1/(m_2-m_1)$ and other masses. Fig. 17 shows the simulated maximal ion flux of MIRACLS' new 30 keV MR-ToF device for $A=132$ and an abundance ratio of 1 as a function of $m_1/(m_2-m_1)$ in comparison to low-energy MR-ToF devices discussed above. In all cases studied the maximal ion flux of MIRACLS' new 30 keV MR-ToF device is significantly larger than the one in existing state-of-the-art MR-ToF devices.

A further increase of maximal ion flux could be envisioned by stacking several ion bunches simultaneously in the MR-ToF apparatus similar to reports of stacking different ion species [68] or by a further optimization of the operational parameters (e.g. by studying the influence of the in-trap lift potential in more depth). When there are two or more different species of contaminants with quite different mass ratios $m_1/(m_2-m_1)$, 2-step MR-ToF cleaning could allow a larger ion flux. Such a 2-step MR-ToF cleaning could become possible by mass selective retrapping in a dedicated Paul trap [14,62,63] or by beam cleaning with the deflector electrodes during the first few revolutions of one measurement cycle [65].

8. Conclusion and outlook

Mass resolving power and space-charge simulations for MR-ToF devices are carried out, and show a good agreement with time-of-flight and collisional-induced fluorescence measurements performed with the MIRACLS low-energy MR-ToF device operating at 1.5 keV beam energy. Building on the successful benchmarking of the simulation approach against the experimental data, simulations with different beam energies and Paul-trap settings are carried out. These suggest that the maximal ion flux can be increased by a factor of 13 to 25 when increasing the kinetic energy of the stored ions in the MR-ToF device from 1.5 keV to 30 keV. Different ion preparation schemes to reduce the temporal ion bunch width resulted in little influence on the maximal ion flux per unit of time. In these scenarios, the gain in MR-ToF processing time is counter-balanced by stronger space-charge effects. Hence, no notable net gain in ion flux is observed. Only when dealing with very short-lived ions, the Paul-trap preparation becomes important. For this case a small initial time spread is preferred in order to reach a given mass resolving power within a storage time shorter than the half life of the ion of interest.

[11] Simulations in the MIRACLS low-energy apparatus show that there is no difference in maximal ion flux irrespective if an abundance ratio of 9 or 0.11 of the 24 u and 24.0096 u ions is chosen. The simulations are performed for $A=24$ and $m_1/(m_2-m_1)=2500$, a buffer-gas temperature of either 300 or 5 K and an extraction field strength of 3.3 V/mm. For the Paul trap in MIRACLS' low-energy setup the tail towards higher ToF values is much less pronounced than for the new MIRACLS Paul trap [49], which is still under commissioning and optimization.

Small initial time spreads can either be achieved by Doppler/sympathetic cooling [34] or cryogenic buffer-gas cooling. An alternative method is increasing the extraction field strength during the ion extraction from the Paul-trap cooler-buncher. However, this approach will lead to a larger energy spread worsening the mass resolving power in the limit of infinite revolutions. Following our simulation studies, for a 30 keV MR-ToF device the energy-spread tolerance is significantly larger than for a 1.5 keV MR-ToF device allowing to reach a mass resolving power exceeding 1e5 with a very large extraction field strength. Hence, when a 30 keV MR-ToF device is coupled to a dedicated Paul trap allowing these very small initial time spreads, a given mass resolving power can be obtained within shorter time than in a 1.5 keV MR-ToF device, also for a room-temperature Paul trap and without compromising the maximal attainable mass resolving power.

Because of this shorter processing time and, even more importantly, its larger ion flux a 30 keV MR-ToF device is a very beneficial tool for mass separation at RIB facilities. For this reason, the discussed simulation code is finally used to reconfigure and optimize MIRACLS' 30 keV MR-ToF design for a high mass resolving power and a large ion-flux. Once constructed and commissioned, this 30 keV setup will serve as a prototype towards a general-purpose mass separator for the ISOLDE community. At this initial stage it is planned to deliver purified beams to PUMA and possibly traveling experiments. Based on the simulation work, this instrument has the prospect of improving the maximal ion flux by a factor of around 70 compared to the MIRACLS 1.5 keV MR-ToF setup or other existing state-of-the-art MR-ToF systems. Ultimately, such an MR-ToF system should be embedded into a wider effort for RIB purification, including also next generation magnetic separators. We envision that at each purification stage, i.e. target, ion source, magnetic separator and finally MR-ToF device the maximal amount of contaminants is suppressed such that a highly purified ion sample is delivered at high ion rates to RIB experiments. Isobarically pure beams with an high ion intensity will be beneficial for virtually all fields of rare isotope science, ranging from fundamental symmetry studies, nuclear structure, astrophysics, material science, production of medical isotopes to rare isotope studies with antimatter.

Declaration of competing interest

The authors declare that they have no known competing financial interests or personal relationships that could have appeared to influence the work reported in this paper.

Data availability

Data will be made available on request.

Acknowledgments

The research leading to these results has received funding from the European Research Council (ERC) under the European Union's Horizon 2020 research and innovation programme under grant agreement No. 679038. The work of F.M.M. has been sponsored by the Wolfgang Gentner Programme of the German Federal Ministry of Education and Research (grant no. 05E18CHA). We are grateful for support of the MIRACLS project from CERN, the ISOLDE Collaboration, and the Max–Planck-Institut für Kernphysik (MPI K) in Heidelberg. This work is supported by the CERN Budget for Knowledge Transfer to Medical Applications and by the Natural Sciences and Engineering Council of Canada (NSERC). TRIUMF receives federal funding via a contribution agreement with the National Research Council of Canada. We thank Mark Bisell, Wouter Gins, Kim Dieter Kreim and Stefan Sailer for sharing their optical ray-tracing codes. Additionally, F.M.M. thanks Moritz Pascal Reiter for fruitful discussions on topics related to this manuscript.

Appendix

If not indicated differently, all the simulations are performed with SIMION, version 8.1. The simulations are performed on four workstations with the processors AMD 2700x, Intel Core i7 8700 K, AMD 3900x and Intel Core i7 6700. The random access memory is 64, 32, 128 and 64 GB, respectively. All the files to perform one full simulation of either the MIRACLS' low-energy setup or the 30 keV setup require a storage space of around 80 GB each. The same storage space is also needed for a full simulation of MIRACLS' 30 keV setup including MIRACLS' new Paul trap. Since SIMION only supports multi-threading during the initial refinement, but not for the simulations of the ion trajectories themselves, many different simulations with different settings are started simultaneously on the different cores of the four workstations. The run times last between a few minutes up to three weeks depending on the storage time in the MR-ToF device, the number of simulated ions, the cooling mechanism in the Paul trap and on whether ion–ion interactions are enabled.

Similar to the discussion in Ref. [45], the simulation is split into different geometrical segments. For the MR-ToF simulations a grid resolution of 0.1 mm/grid unit and a convergence objective of 1e−7 V is chosen, for the Paul trap and ion transport simulations the grid resolution is 0.2 or 0.5 mm/grid unit and the convergence objective is 1e−5 V. For selected simulations it is verified, that a smaller grid resolution or a smaller time step size do not lead to any notable changes on the relevant parameters, such as maximal ion flux or mass resolving power. Note that this point was in particular checked for the simulations with 30 keV beam energy. When going from 0.05 to 0.1 mm/grid unit the simulated mass resolving power remains the same, when going further to 0.2 mm/grid unit it is slightly reduced. The simulated maximal ion flux, however, remains similar for all tested grid resolutions between 0.05 mm/grid unit and 0.5 mm/grid unit. Since computational errors shift the energy of both ion species almost equally, the mass separation and hence maximal ion flux is hardly affected by computational errors as long as $m_1/(m_2 - m_1) \ll R_{\mathrm{inf}}$.

Moreover, a simulation with 1000 interacting ions is leading to the same results as a simulation with 100 interacting ions and a charge repulsion factor of 10 for the selfbunching, dispersive and isochronous mode. Additionally, it is verified that e.g. 100 ions with a charge repulsion factor of 250 lead to the same results as 1000 ions with a charge repulsion factor of 25, as tested for the isochronous and selfbunching mode. Based on the comparison with experimental collision-induced fluorescence data, we conclude that the simulations with up to at least a charge repulsion factor of 250 lead to reliable results.

References

[1] T. Giles, R. Catherall, V. Fedosseev, U. Georg, E. Kugler, J. Lettry, M. Lindroos, The high resolution spectrometer at ISOLDE, Nucl. Instrum. Methods Phys. Res. B 204 (2003) 497–501, 14th International Conference on Electromagnetic Isotope Separators and Techniques Related to their Applications.

[2] C.N. Davids, D. Peterson, A compact high-resolution isobar separator for the CARIBU project, Nucl. Instrum. Methods Phys. Res. B 266 (19) (2008) 4449–4453, Proceedings of the XVth International Conference on Electromagnetic Isotope Separators and Techniques Related to their Applications.

[3] S. Grévy, High intensity ion guides and purification techniques for low energy radioactive ion beams, Nucl. Instrum. Methods Phys. Res. B 376 (2016) 200–206, Proceedings of the XVIIth International Conference on Electromagnetic Isotope Separators and Related Topics (EMIS2015), Grand Rapids, MI, U.S.A., 11-15 May 2015.

[4] T. Kurtukian-Nieto, R. Baartman, B. Blank, T. Chiron, C. Davids, F. Delalee, M. Duval, S. El Abbeir, A. Fournier, D. Lunney, F. Méot, L. Serani, M.-H. Stodel, F. Varenne, H. Weick, SPIRAL2/DESIR high resolution mass separator, Nucl. Instrum. Methods Phys. Res. B 317 (2013) 284–289, XVIth International Conference on ElectroMagnetic Isotope Separators and Techniques Related to their Applications, December 2–7, 2012 at Matsue, Japan.

[5] J. Michaud, P. Alfaurt, A. Balana, B. Blank, L. Daudin, T.K. Nieto, B. Lachacinski, L. Serani, F. Varenne, Status on the DESIR high resolution separator commissioning, 2022, http://dx.doi.org/10.48550/ARXIV.2203.11214, arXiv.

[6] M. Marchetto, F. Ames, R. Baartman, C. Barquest, S. Kiy, T. Planche, S. Saminathan, J. Maloney, S. Brown, M. Corwin, D. Sehayek, J. Laroche, Status of the CANREB high-resolution separator at TRIUMF, Nucl. Instrum. Methods Phys. Res. B 463 (2020) 227–231.

[7] A. Piechaczek, V. Shchepunov, H.K. Carter, J.C. Batchelder, E.F. Zganjar, S.N. Liddick, H. Wollnik, Y. Hu, B.O. Griffith, Development of a high resolution isobar separator for study of exotic decays, Nucl. Instrum. Methods Phys. Res. B 266 (19) (2008) 4510–4514.

[8] W.R. Plaß, T. Dickel, U. Czok, H. Geissel, M. Petrick, K. Reinheimer, C. Scheidenberger, M.I. Yavor, Isobar separation by time-of-flight mass spectrometry for low-energy radioactive ion beam facilities, Nucl. Instrum. Methods Phys. Res. B 266 (19–20) (2008) 4560–4564.

[9] P. Schury, K. Okada, S. Shchepunov, T. Sonoda, A. Takamine, M. Wada, H. Wollnik, Y. Yamazaki, Multi-reflection time-of-flight mass spectrograph for short-lived radioactive ions, Eur. Phys. J. A 42 (3) (2009) 343.

[10] F. Wienholtz, D. Beck, K. Blaum, C. Borgmann, M. Breitenfeldt, R.B. Cakirli, S. George, F. Herfurth, J.D. Holt, M. Kowalska, S. Kreim, D. Lunney, V. Manea, J. Menéndez, D. Neidherr, M. Rosenbusch, L. Schweikhard, A. Schwenk, J. Simonis, J. Stanja, R.N. Wolf, K. Zuber, Masses of exotic calcium isotopes pin down nuclear forces, Nature 498 (7454) (2013) 346–349.

[11] R.N. Wolf, D. Beck, K. Blaum, C. Böhm, C. Borgmann, M. Breitenfeldt, F. Herfurth, A. Herlert, M. Kowalska, S. Kreim, D. Lunney, S. Naimi, D. Neidherr, M. Rosenbusch, L. Schweikhard, J. Stanja, F. Wienholtz, K. Zuber, On-line separation of short-lived nuclei by a multi-reflection time-of-flight device, Nucl. Instrum. Methods Phys. Res. A 686 (2012) 82–90.

[12] R. Wolf, F. Wienholtz, D. Atanasov, D. Beck, K. Blaum, C. Borgmann, F. Herfurth, M. Kowalska, S. Kreim, Y.A. Litvinov, D. Lunney, V. Manea, D. Neidherr, M. Rosenbusch, L. Schweikhard, J. Stanja, K. Zuber, ISOLTRAP's multi-reflection time-of-flight mass separator/spectrometer, Int. J. Mass Spectrom. 349–350 (2013) 123–133, 100 years of Mass Spectrometry.

[13] T. Dickel, W. Plaß, A. Becker, U. Czok, H. Geissel, E. Haettner, C. Jesch, W. Kinsel, M. Petrick, C. Scheidenberger, A. Simon, M. Yavor, A high-performance multiple-reflection time-of-flight mass spectrometer and isobar separator for the research with exotic nuclei, Nucl. Instrum. Methods Phys. Res. A 777 (2015) 172–188.

[14] M. Reiter, S.A.S. Andrés, J. Bergmann, T. Dickel, J. Dilling, A. Jacobs, A. Kwiatkowski, W. Plaß, C. Scheidenberger, D. Short, C. Will, C. Babcock, E. Dunling, A. Finlay, C. Hornung, C. Jesch, R. Klawitter, B. Kootte, D. Lascar, E. Leistenschneider, T. Murböck, S. Paul, M. Yavor, Commissioning and performance of TITAN's multiple-reflection time-of-flight mass-spectrometer and isobar separator, Nucl. Instrum. Methods Phys. Res. A 1018 (2021) 165823.

[15] P. Chauveau, P. Delahaye, G. De France, S. El Abir, J. Lory, Y. Merrer, M. Rosenbusch, L. Schweikhard, R. Wolf, PILGRIM, a multi-reflection time-of-flight mass spectrometer for spiral2-S3 at GANIL, Nucl. Instrum. Methods Phys. Res. B 376 (2016) 211–215, Proceedings of the XVIIth International Conference on Electromagnetic Isotope Separators and Related Topics (EMIS2015), Grand Rapids, MI, U.S.A., 11-15 May 2015.

[16] B. Liu, M. Brodeur, D. Burdette, J. Kelly, T. Kim, J. Long, P. O'Malley, The performance of the commissioned Notre Dame multi-reflection time-of-flight mass spectrometer, Nucl. Instrum. Methods Phys. Res. A 985 (2021) 164679.

[17] M. Rosenbusch, M. Wada, S. Chen, A. Takamine, S. Iimura, D. Hou, W. Xian, S. Yan, P. Schury, Y. Hirayama, Y. Ito, H. Ishiyama, S. Kimura, T. Kojima, J. Lee, J. Liu, S. Michimasa, H. Miyatake, J. Moon, M. Mukai, S. Nishimura, S. Naimi, T. Niwase, T. Sonoda, Y. Watanabe, H. Wollnik, The new MRTOF mass spectrograph following the zerodegree spectrometer at RIKEN's RIBF facility, Nucl. Instrum. Methods Phys. Res. A (2022) 167824.

[18] H.B. Pedersen, D. Strasser, S. Ring, O. Heber, M.L. Rappaport, Y. Rudich, I. Sagi, D. Zajfman, Ion motion synchronization in an ion-trap resonator, Phys. Rev. Lett. 87 (2001) 055001.

[19] D. Zajfman, O. Heber, M.L. Rappaport, H.B. Pedersen, D. Strasser, S. Goldberg, Self-bunching effect in an ion trap resonator, J. Opt. Soc. Amer. B 20 (5) (2003) 1028–1032.

[20] H.B. Pedersen, D. Strasser, B. Amarant, O. Heber, M.L. Rappaport, D. Zajfman, Diffusion and synchronization in an ion-trap resonator, Phys. Rev. A 65 (2002) 042704.

[21] D. Strasser, T. Geyer, H.B. Pedersen, O. Heber, S. Goldberg, B. Amarant, A. Diner, Y. Rudich, I. Sagi, M. Rappaport, D.J. Tannor, D. Zajfman, Negative mass instability for interacting particles in a 1D box: Theory and application, Phys. Rev. Lett. 89 (2002) 283204.

[22] P. Bolotskikh, D. Grinfeld, A. Makarov, M. Monastyrskiy, Coulomb dynamics of ion bunches in multi-reflection electrostatic traps, Nucl. Instrum. Methods Phys. Res. A 645 (1) (2011) 146–152, The Eighth International Conference on Charged Particle Optics.

[23] M.W. Froese, M. Lange, S. Menk, M. Grieser, O. Heber, F. Laux, R. Repnow, T. Sieber, Y. Toker, R. von Hahn, A. Wolf, K. Blaum, The decay of ion bunches in the self-bunching mode, New J. Phys. 14 (7) (2012) 073010.

[24] S. Lechner, P. Fischer, H. Heylen, V. Lagaki, F. Maier, P. Plattner, M. Rosenbusch, S. Sels, F. Wienholtz, R.N. Wolf, W. Nörtershäuser, L. Schweikhard, S. Malbrunot-Ettenauer, Fluorescence detection as a new diagnostics tool for electrostatic ion beam traps, Hyperfine Interact. 240 (1) (2019) 95.

[25] D. Gupta, R. Singh, R. Ringle, C.R. Nicoloff, I. Rahinov, O. Heber, D. Zajfman, Particle-in-cell techniques for the study of space charge effects in an electrostatic ion beam trap, Phys. Rev. E 104 (2021) 065202.

[26] M. Rosenbusch, S. Kemnitz, R. Schneider, L. Schweikhard, R. Tschiersch, R.N. Wolf, Towards systematic investigations of space-charge phenomena in multi-reflection ion traps, AIP Conf. Proc. 1521 (1) (2013) 53–62.

[27] M. Rosenbusch, P. Chauveau, P. Delahaye, G. Marx, L. Schweikhard, F. Wienholtz, R.N. Wolf, Delayed bunching for multi-reflection time-of-flight mass separation, AIP Conf. Proc. 1668 (1) (2015) 050001.

[28] T. Aumann, W. Bartmann, O. Boine-Frankenheim, A. Bouvard, A. Broche, F. Butin, D. Calvet, J. Carbonell, P. Chiggiato, H. De Gersem, R. De Oliveira, T. Dobers, F. Ehm, J.F. Somoza, J. Fischer, M. Fraser, E. Friedrich, A. Frotscher, M. Gomez-Ramos, J.-L. Grenard, A. Hobl, G. Hupin, A. Husson, P. Indelicato, K. Johnston, C. Klink, Y. Kubota, R. Lazauskas, S. Malbrunot-Ettenauer, N. Marsic, W.F. O Müller, S. Naimi, N. Nakatsuka, R. Necca, D. Neidherr, G. Neyens, A. Obertelli, Y. Ono, S. Pasinelli, N. Paul, E.C. Pollacco, D. Rossi, H. Scheit, M. Schlaich, A. Schmidt, L. Schweikhard, R. Seki, S. Sels, E. Siesling, T. Uesaka, M. Vilén, M. Wada, F. Wienholtz, S. Wycech, S. Zacarias, PUMA, antiproton unstable matter annihilation, Eur. Phys. J. A 58 (5) (2022) 88.

[29] C. Müller, K. Zhernosekov, U. Köster, K. Johnston, H. Dorrer, A. Hohn, N.T. van der Walt, A. Türler, R. Schibli, A unique matched quadruplet of terbium radioisotopes for PET and SPECT and for α- and β- radionuclide therapy: An in Vivo proof-of-concept study with a new receptor-targeted folate derivative, J. Nucl. Med. 53 (12) (2012) 1951–1959.

[30] C. Müller, C. Vermeulen, K. Johnston, U. Köster, R. Schmid, A. Türler, N.P. van der Meulen, Preclinical in Vivo application of 152Tb-DOTANOC: A radiolanthanide for PET imaging, EJNMMI Research 6 (1) (2016) 35.

[31] F.M. Maier, P. Fischer, H. Heylen, V. Lagaki, S. Lechner, P. Plattner, S. Sels, F. Wienholtz, W. Nörtershäuser, L. Schweikhard, S. Malbrunot-Ettenauer, Simulations of a proof-of-principle experiment for collinear laser spectroscopy within a multi-reflection time-of-flight device, Hyperfine Interact. 240 (1) (2019) 54.

[32] K. Kreim, M. Bissell, J. Papuga, K. Blaum, M.D. Rydt, R.G. Ruiz, S. Goriely, H. Heylen, M. Kowalska, R. Neugart, G. Neyens, W. Nörtershäuser, M. Rajabali, R.S. Alarcón, H. Stroke, D. Yordanov, Nuclear charge radii of potassium isotopes beyond N=28, Phys. Lett. B 731 (2014) 97–102.

[33] K. Kreim, Collinear Laser Spectroscopy of Potassium, (Ph.D. thesis), University Heidelberg, 2013.

[34] S. Sels, F.M. Maier, M. Au, P. Fischer, C. Kanitz, V. Lagaki, S. Lechner, E. Leistenschneider, D. Leimbach, E.M. Lykiardopoulou, A.A. Kwiatkowski, T. Manovitz, Y.N. Vila Gracia, G. Neyens, P. Plattner, S. Rothe, L. Schweikhard, M. Vilen, R.N. Wolf, S. Malbrunot-Ettenauer, Doppler and sympathetic cooling for the investigation of short-lived radioactive ions, Phys. Rev. Res. 4 (2022) 033229.

[35] S. Sels, P. Fischer, H. Heylen, V. Lagaki, S. Lechner, F. Maier, P. Plattner, M. Rosenbusch, F. Wienholtz, R. Wolf, W. Nörtershäuser, L. Schweikhard, S. Malbrunot-Ettenauer, First steps in the development of the multi ion reflection apparatus for collinear laser spectroscopy, Nucl. Instrum. Methods Phys. Res. B 463 (2020) 310–314.

[36] V. Lagaki, H. Heylen, I. Belosevic, P. Fischer, C. Kanitz, S. Lechner, F. Maier, W. Nörtershäuser, P. Plattner, M. Rosenbusch, S. Sels, L. Schweikhard, M. Vilen, F. Wienholtz, R. Wolf, S. Malbrunot-Ettenauer, An accuracy benchmark of the MIRACLS apparatus: Conventional, single-passage collinear laser spectroscopy inside a MR-ToF device, Nucl. Instrum. Methods Phys. Res. A 1014 (2021) 165663.

[37] T. Beyer, K. Blaum, M. Block, C.E. Düllmann, K. Eberhardt, M. Eibach, N. Frömmgen, C. Geppert, C. Gorges, J. Grund, M. Hammen, S. Kaufmann, A. Krieger, S. Nagy, W. Nörterhäuser, D. Renisch, C. Smorra, E. Will, An RFQ cooler and buncher for the TRIGA-SPEC experiment, Appl. Phys. B 114 (1) (2014) 129–136.

[38] R.N. Wolf, G. Marx, M. Rosenbusch, L. Schweikhard, Static-mirror ion capture and time focusing for electrostatic ion-beam traps and multi-reflection time-of-flight mass analyzers by use of an in-trap potential lift, Int. J. Mass Spectrom. 313 (2012) 8–14.

[39] T. Dickel, M.I. Yavor, J. Lang, W.R. Plaß, W. Lippert, H. Geissel, C. Scheidenberger, Dynamical time focus shift in multiple-reflection time-of-flight mass spectrometers, Int. J. Mass Spectrom. 412 (2017) 1–7.

[40] V. Lagaki, P. Fischer, H. Heylen, F. Hummer, S. Lechner, S. Sels, F. Maier, P. Plattner, M. Rosenbusch, F. Wienholtz, R. Wolf, W. Nörtershäuser, L. Schweikhard, S. Malbrunot-Ettenauer, Stray-light suppression for the MIRACLS proof-of-principle experiment, Acta Phys. Polon. B 51 (2020) 571–576.

[41] T. Murböck, S. Schmidt, Z. Andelkovic, G. Birkl, W. Nörtershäuser, M. Vogel, A compact source for bunches of singly charged atomic ions, Rev. Sci. Instrum. 87 (4) (2016) 043302.

[42] F. Wienholtz, K. Blaum, J. Karthein, D. Lunney, S. Malbrunot-Ettenauer, V. Manea, M. Mougeot, L. Schweikhard, T. Steinsberger, R. Wolf, Improved stability of multi-reflection time-of-flight mass spectrometers through passive and active voltage stabilization, Nucl. Instrum. Methods Phys. Res. B 463 (2020) 348–356.

[43] P. Fischer, L. Schweikhard, Multiple active voltage stabilizations for multi-reflection time-of-flight mass spectrometry, Rev. Sci. Instrum. 92 (6) (2021) 063203.

[44] D. Manura, SIMION HS1 collision model REV4, 2007.
[45] F. Maier, M. Vilen, I. Belosevic, F. Buchinger, C. Kanitz, S. Lechner, E. Leistenschneider, W. Nörtershäuser, P. Plattner, L. Schweikhard, S. Sels, F. Wienholtz, S. Malbrunot-Ettenauer, Simulation studies of a 30-keV MR-ToF device for highly sensitive collinear laser spectroscopy, Nucl. Instrum. Methods Phys. Res. A 1048 (2023) 167927.
[46] Y. Tian, Y. Wang, J. Wang, X. Zhou, W. Huang, Designing a multi-reflection time-of-flight mass analyzer for LPT, Int. J. Mass Spectrom. 408 (2016) 28–32.
[47] D. Manura, SIMION simplex optimizer, 2007.
[48] S. Schwarz, G. Bollen, R. Ringle, J. Savory, P. Schury, The LEBIT ion cooler and buncher, Nucl. Instrum. Methods Phys. Res. A 816 (2016) 131–141.
[49] C. Kanitz, Construction and characterization of a Paul trap for laser spectroscopy of exotic radionuclides in an MR-ToF device, M.Sc. thesis, Friedrich-Alexander-University Erlangen-Nürnberg, 2019.
[50] A. Verenchikov, M.I. Yavor, T.V. Pomozov, Electrostatic ion mirrors, 2016, Google Patents, US Patent 9, 396, 922 B2.
[51] M. Yavor, N. Gall, M. Muradymov, T. Pomozov, I. Kurnin, A. Monakov, A. Arsenev, Y.T. Oganessian, A. Karpov, A. Rodin, L. Krupa, T. Dickel, W. Plaß, C. Scheidenberger, Development of a mass spectrometer for high-precision mass measurements of superheavy elements at JINR, J. Instrum. 17 (11) (2022) P11033.
[52] W.R. Plaß, T. Dickel, S.A.S. Andres, J. Ebert, F. Greiner, C. Hornung, C. Jesch, J. Lang, W. Lippert, T. Majoros, D. Short, H. Geissel, E. Haettner, M.P. Reiter, A.-K. Rink, C. Scheidenberger, M.I. Yavor, High-performance multiple-reflection time-of-flight mass spectrometers for research with exotic nuclei and for analytical mass spectrometry, Phys. Scr. T166 (2015) 014069.
[53] S. Sailer, Improvements of the Optical Detection Setup for Collinear Laser Spectroscopy of Short-Lived Radioactive Nuclides and Spectroscopic Studies on the Hyperfine Parameters of ^{208}Bi, (M.Sc. thesis), TU Munich, 2016.
[54] W. Gins, Development of a dedicated laser-polarization beamline for ISOLDE-CERN, (Ph.D. thesis), KU Leuven, 2019.
[55] F. Hummer, Investigation of Space Charge Effects in MIRACLS' Proof-of- Principle MR-ToF Device, B.Sc. thesis, Johannes Kepler University Linz, 2019.
[56] D. Manura, SIMION charge repulsion, 2007.
[57] A. Nieminen, P. Campbell, J. Billowes, D. Forest, J. Griffith, J. Huikari, A. Jokinen, I. Moore, R. Moore, G. Tungate, J. Äystö, Cooling and bunching of ion beams for collinear laser spectroscopy, Nucl. Instrum. Methods Phys. Res. B 204 (2003) 563–569, 14th International Conference on Electromagnetic Isotope Separators and Techniques Related to their Applications.
[58] B. Barquest, G. Bollen, P. Mantica, K. Minamisono, R. Ringle, S. Schwarz, C. Sumithrarachchi, RFQ beam cooler and buncher for collinear laser spectroscopy of rare isotopes, Nucl. Instrum. Methods Phys. Res. A 866 (2017) 18–28.
[59] S. Van Gorp, M. Beck, M. Breitenfeldt, V. De Leebeeck, P. Friedag, A. Herlert, T. Iitaka, J. Mader, V. Kozlov, S. Roccia, G. Soti, M. Tandecki, E. Traykov, F. Wauters, C. Weinheimer, D. Zákoucký, N. Severijns, Simbuca, using a graphics card to simulate coulomb interactions in a penning trap, Nucl. Instrum. Methods Phys. Res. A 638 (1) (2011) 192–200.
[60] R. Hipple, S. Lund, Modeling of space-charge effects in the oriss mrtof device for applications to FRIB, in: Proc. NAPAC'19, no. 4, in: North American Particle Accelerator Conference, JACoW Publishing, Geneva, Switzerland, 2019, pp. 786–788, DOI: 10.18429/JACoW-NAPAC2019-WEPLS10.
[61] Personal Communications with Frank Wienholtz, ISOLTRAP collaboration, 2018.
[62] C. Izzo, J. Bergmann, K.A. Dietrich, E. Dunling, D. Fusco, A. Jacobs, B. Kootte, G. Kripkó-Koncz, Y. Lan, E. Leistenschneider, E.M. Lykiardopoulou, I. Mukul, S.F. Paul, M.P. Reiter, J.L. Tracy, C. Andreoiu, T. Brunner, T. Dickel, J. Dilling, I. Dillmann, G. Gwinner, D. Lascar, K.G. Leach, W.R. Plaß, C. Scheidenberger, M.E. Wieser, A.A. Kwiatkowski, Mass measurements of neutron-rich indium isotopes for *r*-process studies, Phys. Rev. C 103 (2021) 025811.
[63] S.F. Paul, J. Bergmann, J.D. Cardona, K.A. Dietrich, E. Dunling, Z. Hockenbery, C. Hornung, C. Izzo, A. Jacobs, A. Javaji, B. Kootte, Y. Lan, E. Leistenschneider, E.M. Lykiardopoulou, I. Mukul, T. Murböck, W.S. Porter, R. Silwal, M.B. Smith, J. Ringuette, T. Brunner, T. Dickel, I. Dillmann, G. Gwinner, M. MacCormick, M.P. Reiter, H. Schatz, N.A. Smirnova, J. Dilling, A.A. Kwiatkowski, Mass measurements of $^{60-63}$Ga reduce x-ray burst model uncertainties and extend the evaluated $T = 1$ isobaric multiplet mass equation, Phys. Rev. C 104 (2021) 065803.
[64] Open-source, WARP: Open-source particle-in-cell Python package, 2022.
[65] P. Fischer, S. Knauer, G. Marx, L. Schweikhard, In-depth study of in-trap high-resolution mass separation by transversal ion ejection from a multi-reflection time-of-flight device, Rev. Sci. Instrum. 89 (1) (2018) 015114.
[66] F. Wienholtz, S. Kreim, M. Rosenbusch, L. Schweikhard, R. Wolf, Mass-selective ion ejection from multi-reflection time-of-flight devices via a pulsed in-trap lift, Int. J. Mass Spectrom. 421 (2017) 285–293.
[67] N.E. Bradbury, R.A. Nielsen, Absolute values of the electron mobility in hydrogen, Phys. Rev. 49 (1936) 388–393.
[68] P. Fischer, G. Marx, L. Schweikhard, Multiple ion capture and separation in an electrostatic storage device, Int. J. Mass Spectrom. 435 (2019) 305–314.